Ann Nucl Med
DOI 10.1007/s12149-009-0243-7

ORIGINAL ARTICLE

Influence of residual oxygen-15-labeled carbon monoxide radioactivity on cerebral blood flow and oxygen extraction fraction in a dual-tracer autoradiographic method

Katsuhiro Iwanishi · Hiroshi Watabe · Takuya Hayashi · Yoshinori Miyake · Kotaro Minato · Hidehiro Iida

Received: 14 December 2008 / Accepted: 8 January 2009

Abstract
Objective Cerebral blood flow (CBF), cerebral metabolic rate of oxygen ($CMRO_2$), oxygen extraction fraction (OEF), and cerebral blood volume (CBV) are quantitatively measured with PET with ^{15}O gases. Kudomi et al. developed a dual tracer autoradiographic (DARG) protocol that enables the duration of a PET study to be shortened by sequentially administrating $^{15}O_2$ and $C^{15}O_2$ gases. In this protocol, before the sequential PET scan with $^{15}O_2$ and $C^{15}O_2$ gases ($^{15}O_2$–$C^{15}O_2$ PET scan), a PET scan with $C^{15}O$ should be preceded to obtain CBV image. $C^{15}O$ has a high affinity for red blood cells and a very slow washout rate, and residual radioactivity from $C^{15}O$ might exist during a $^{15}O_2$–$C^{15}O_2$ PET scan. As the current DARG method assumes no residual $C^{15}O$ radioactivity before scanning, we performed computer simulations to evaluate the influence of the residual $C^{15}O$ radioactivity on the accuracy of measured CBF and OEF values with DARG method and also proposed a subtraction technique to minimize the error due to the residual $C^{15}O$ radioactivity.
Methods In the simulation, normal and ischemic conditions were considered. The $^{15}O_2$ and $C^{15}O_2$ PET count curves with the residual $C^{15}O$ PET counts were generated by the arterial input function with the residual $C^{15}O$ radioactivity. The amounts of residual $C^{15}O$ radioactivity were varied by changing the interval between the $C^{15}O$ PET scan and $^{15}O_2$–$C^{15}O_2$ PET scan, and the absolute inhaled radioactivity of the $C^{15}O$ gas. Using the simulated input functions and the PET counts, the CBF and OEF were computed by the DARG method. Furthermore, we evaluated a subtraction method that subtracts the influence of the $C^{15}O$ gas in the input function and PET counts.
Results Our simulations revealed that the CBF and OEF values were underestimated by the residual $C^{15}O$ radioactivity. The magnitude of this underestimation depended on the amount of $C^{15}O$ radioactivity and the physiological conditions. This underestimation was corrected by the subtraction method.
Conclusions This study showed the influence of $C^{15}O$ radioactivity in DARG protocol, and the magnitude of the influence was affected by several factors, such as the radioactivity of $C^{15}O$, and the physiological condition.

Keywords PET · OEF · CBV · Carbon monoxide

K. Iwanishi (✉) · H. Watabe · T. Hayashi · H. Iida
Department of Investigative Radiology, National Cardiovascular Center Research Institute, 5-7-1 Fujishirodai, Suita, Osaka 565-8565, Japan
e-mail: kiwanish@ri.ncvc.go.jp

Y. Miyake
Department of Radiology and Nuclear Medicine, National Cardiovascular Center, Osaka, Japan

K. Iwanishi · K. Minato
Infomatics Science, Nara Institute of Science and Technology, Nara, Japan

Introduction

Positron emission tomography with ^{15}O gas can quantitatively measure cerebral blood flow (CBF), oxygen extraction fraction (OEF), cerebral metabolic rate of oxygen ($CMRO_2$), and cerebral blood volume (CBV). These functional values are important clinical indices that can be used to evaluate ischemic degree mainly in chronic cerebral arterial occlusive diseases. Several quantitative approaches

Published online: 10 April 2009

have been developed to obtain CBF and $CMRO_2$ images based on a single-tissue compartment model for oxygen and water kinetics [1–4]. In the steady-state method [5–9], quantitative images are estimated from data acquired while in the steady state reached during the continuous inhalation of $^{15}O_2$ and $C^{15}O_2$. The study period with this method is long (approximately 2 h) due to the waiting time needed to reach equilibrium. The autoradiographic method, which uses separate administrations of three traces of CO, CO_2, and O_2 (three-step ARG), has also been employed [3, 10–14]. The study period with the ARG method is shorter than that need with the steady-state method. However, a study with the ARG method still takes more than half an hour, because there is a waiting time for the decay of the residual radioactivity of the preceding tracer used.

Previously, Kudomi et al. developed a dual tracer autoradiographic (DARG) method to shorten the PET study period [15, 16]. This method used a single PET scan with sequential administration of dual tracers of $^{15}O_2$ and $C^{15}O_2$ ($^{15}O_2$–$C^{15}O_2$ scan), and computed CBF and $CMRO_2$ simultaneously in an autoradiographic manner. Although the DARG approach eliminated the waiting time of radioactivity decay between $^{15}O_2$ and $C^{15}O_2$ administrations, a separate PET scan with $C^{15}O$ is required for obtaining a CBV image and correction of blood volume in $CMRO_2$ before the DARG scan. However, between these scans for $C^{15}O$ and the DARG we need another waiting time for the radioactivity decay of $C^{15}O$, since the DARG approach itself does not take into account the residual $C^{15}O$ radioactivity in the arterial input function (AIF) and PET data. Furthermore, CO has a relatively long biological clearance from the blood due to high affinity to hemoglobin. While it is desired to further decrease the waiting time for the decay in the actual clinical study, it has not been defined how long it should be, and how small amount of the residual activity will affect the accuracy of CBF and $CMRO_2$.

In this study, we performed computer simulations and evaluated the influence of this residual $C^{15}O$ radioactivity on the CBF and OEF values obtained by the DARG method. Moreover, we proposed a method to remove the influence of the $C^{15}O$ on the DARG method calculation (Subtraction method).

Materials and methods

Computation of functional values

CBF and OEF values were calculated from tissue TAC [$C_i(t)$] and AIF during an $^{15}O_2$–$C^{15}O_2$ scan, based on a single-tissue compartment model for oxygen and water, and the DARG method [15]. Using the method developed by Kudomi et al. [16], the AIF was separated into $^{15}O_2$ ($A_{O_2}(t)$) and $H_2^{15}O$ ($A_{H_2O}(t)$) (Note that although we used $C^{15}O_2$ gas, we used $H_2^{15}O$ for the expression in this section due to the rapid exchange of $H_2^{15}O$ by carbonate dehydratase in the lung). The total radioactivity in the tissue after the $^{15}O_2$ and $C^{15}O_2$ administration can be expressed as,

$$Ci(t) = f \cdot A_{H_2O}(t) \otimes \exp^{-\frac{f}{p}t} + E \cdot f \cdot A_{O_2}(t) \otimes \exp^{-\frac{f}{p}t} + V_B \cdot R_{Hct}(1 - Fv \cdot E) A_{O_2}(t) \quad (1)$$

where f is CBF, E is the OEF, p is the blood/tissue partition coefficient of water, R_{Hct} is the small-to-large vessel hematocrit ratio, and V_B is the cerebral blood volume. F_v is the effective venous fraction. The first term of the right-hand side describes the amount of water entering the tissue. The second term represents the amount of oxygen that enters the tissue and is immediately metabolized to water. The third term is the radioactivity of the $^{15}O_2$ in the blood vessels.

V_B is separately calculated using data from a $C^{15}O$ scan and the following equation [13]:

$$V_B = \frac{C_{CO}}{R_{Hct} \cdot \rho_{brain} \cdot RI_{CO} \cdot \rho_{blood}}. \quad (2)$$

ρ_{brain} and ρ_{blood} represent the densities of blood (=1.06 g/mL) and brain tissue (=1.04 g/mL). RI_{CO} (Bq/mL) is the mean of the radioactivity concentration for $C^{15}O$ in the arterial blood.

To calculate functional values using a look-up table procedure, Eq. 1 was integrated for the periods after the $H_2^{15}O$ (represents $\int_W$) and $^{15}O_2$ administration (represents $\int_O$) as

$$\begin{aligned}
\int_w Ci(t)dt &= f \int_w A_{H_2O}(t) \otimes \exp^{-\frac{f}{p}t} dt \\
&\quad + E \cdot f \int_w A_{O_2}(t) \otimes \exp^{-\frac{f}{p}t} dt + V_B \\
&\quad \cdot R_{Hct}(1 - Fv \cdot E) \int_w A_{O_2}(t)dt \\
\int_o Ci(t)dt &= f \int_o A_{H_2O}(t) \otimes \exp^{-\frac{f}{p}t} dt \\
&\quad + E \cdot f \int_o A_{O_2}(t) \otimes \exp^{-\frac{f}{p}t} dt + V_B \\
&\quad \cdot R_{Hct}(1 - Fv \cdot E) \int_o A_{O_2}(t)dt
\end{aligned} \quad (3)$$

From the above equation, E can be expressed as follows:

$$E = \frac{\int_o Ci(t) - f \int_o A_{H_2O} \otimes \exp^{-\frac{f}{p}t} dt - V_B \cdot R_{Hct} \int_o A_{O_2} dt}{f \int_o A_{O_2} \otimes \exp^{-\frac{f}{p}t} dt - V_B \cdot R_{Hct} \cdot Fv \int_o A_{O_2} dt}. \quad (4)$$

Substituting Eq. 4 into Eq. 3, we obtain

$$\int_w \mathrm{Ci}(t)\mathrm{d}t = f\int_w A_{\mathrm{H_2O}}(t)\otimes\exp^{-\frac{f}{P}t}\mathrm{d}t + V_\mathrm{B}\cdot R_\mathrm{Hct}\int_w A_{\mathrm{O_2}}(t)\mathrm{d}t + \left(f\int_w A_{\mathrm{O_2}}(t)\otimes\exp^{-\frac{f}{P}t}\mathrm{d}t - V_\mathrm{B}\cdot R_\mathrm{Hct}\cdot \mathrm{Fv}\int_w A_{\mathrm{O_2}}(t)\mathrm{d}t\right) \times \frac{\int_o \mathrm{Ci}(t) - f\int_o A_{\mathrm{H_2O}}\otimes\exp^{-\frac{f}{P}t}\mathrm{d}t - V_\mathrm{B}\cdot R_\mathrm{Hct}\int_o A_{\mathrm{O_2}}\mathrm{d}t}{f\int_o A_{\mathrm{O_2}}\otimes\exp^{-\frac{f}{P}t}\mathrm{d}t - V_\mathrm{B}\cdot R_\mathrm{Hct}\cdot \mathrm{Fv}\int_o A_{\mathrm{O_2}}\mathrm{d}t}. \quad (5)$$

Using Eq. 5, f can be estimated using a look-up table procedure based on the integration value of the tissue TAC and separated input function. Next, E can be calculated using Eq. 4.

Study protocol with DARG method

Figure 1 shows a schematic diagram of the clinical study protocol with the DARG method for our institute. The PET scanner we used was an ECAT EXACT47 (CTI Inc., Knoxville, USA). First, a 10 min transmission scan was performed to correct for gamma ray attenuation. Then gaseous $C^{15}O$ of 2500 MBq was inhaled for 30 s, and 90 s post-inhalation, a 4 min emission scan ($C^{15}O$ scan) was performed to obtain a CBV image. Finally, a single dynamic PET scan was conducted during the sequential administration of gaseous $^{15}O_2$ (4000 MBq) and $C^{15}O_2$ (5000 MBq) in a short time interval. Their inhalation times were 1 min.

A catheter was inserted into the brachial artery of the patient. The arterial blood was sampled at the beginning of the $C^{15}O$ scan for 30 s and the radioactivity concentration in the arterial blood was measured by a Well counter system (Shimadzu Corporation, Kyoto, JAPAN). In order to obtain the AIF, the radioactivity in the arterial blood during a $^{15}O_2$–$C^{15}O_2$ scan was continuously monitored by a GSO detector [17] with a flow rate of 3.5 mL/min. The inner diameter of the tube was approximately 2 mm, and the distance from the catheter to the detector was 20–25 cm.

Residual $C^{15}O$ radioactivity

As described in the "Introduction", the AIF and PET counts obtained during a DARG study may be contaminated by residual $C^{15}O$ radioactivity. By assuming that the $C^{15}O$ was physically decayed but not biologically cleared, the radioactivity of the $C^{15}O$ in the AIF and PET counts during the O_2–CO_2 scan could be quantified. The residual radioactivity of the $C^{15}O$ [$R_{CO}(0)$ (Bq/mL)] in the AIF at the start time of the O_2–CO_2 can be written as follows:

$$R_\mathrm{CO} = A_\mathrm{CO}\cdot\exp(-\lambda T), \quad (6)$$

where A_{CO} (Bq/mL) is the measured arterial radioactivity for $C^{15}O$ by the Well counter and λ is the physical decay constant for ^{15}O (0.005670 s^{-1}).

PET counts from the residual $C^{15}O$ (C_{CO}) were calculated from R_{CO} and the measured CBV (V_B) by $C^{15}O$ scan from Eq. 2 as follows

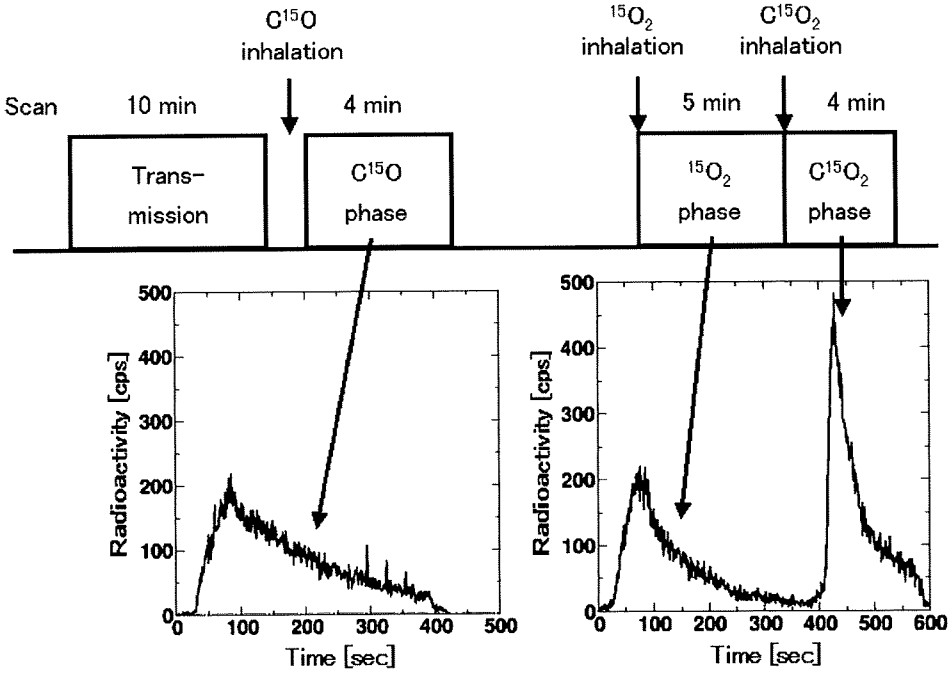

Fig. 1 Schematic diagram of PET study with DARG method protocol. After a 10 min transmission scan, $C^{15}O$ gas is inhaled for 30 s before the start of a 4 min scan. There is approximately 10 min in the administration interval for $C^{15}O$ and $^{15}O_2$. Next, a 9 min single scan with sequential administration of $^{15}O_2$ and $C^{15}O_2$ is performed. The administration interval between $^{15}O_2$ and $C^{15}O_2$ is 300 s. The graphs below are arterial input functions without corrections for decay, delay, and scaling for $C^{15}O$ (*left*), $^{15}O_2$ and $C^{15}O_2$ (*right*)

$$C_{CO} = R_{CO} \cdot \rho_{blood} \cdot \rho_{brain} \cdot R_{Hct} \cdot V_B. \quad (7)$$

We proposed a subtraction method that eliminates the influence of the $C^{15}O$ radioactivity in both the AIF and PET counts during the O_2–CO_2 scan. The true AIF (A_{True}) of the $^{15}O_2$–$C^{15}O_2$ at time t was obtained by subtracting R_{CO} from the measured whole radioactivity [$A_{whole}(t)$], i.e.,

$$A_{True}(t) = A_{Whole}(t) - R_{CO}. \quad (8)$$

Note that $A_{True}(t)$ and $A_{Whole}(t)$ were corrected for the physical decay of ^{15}O against the scan start time 0. PET counts without the residual CO radioactivity could be obtained by subtracting C_{co} in Eq. (7) from the observed PET counts as follows:

$$C_{True}(t) = C_i(t) - C_{co}. \quad (9)$$

Using $A_{True}(t)$ and $C_{True}(t)$, CBF and OEF were calculated in the DARG manner.

Simulation studies

As shown in Eq. 1, DARG calculation does not take into count the residual radioactivity of the CO. However, in an actual situation, both the PET count [Ci(t)] and the input function (A_{O_2} and A_{H_2O}) might contain radioactivity from the $C^{15}O$. So, the CBF and OEF values calculated by the DARG method are influenced by the $C^{15}O$ radioactivity, causing error and noise in the terms of Eq. 1. Computer simulations were performed to evaluate this influence. Both normal and ischemic models were considered in these simulations. Moreover, the effect of the subtraction method was examined.

The simulations were performed using a PC [CPU: Intel (R) Pentium (R) 4 2.80 GHz, OS: Linux Fedora Core 7] with a PyBLD environment [18].

Simulated input function with CO radioactivity

We used a typical arterial input function from one patient's data for the simulations. From the measured input function, the input functions with $C^{15}O$ radioactivity (combined input function, CIF) were generated using Eq. 6. The amount of residual $C^{15}O$ radioactivity was varied by changing two conditions, the time lag between the $C^{15}O$ scan and the $^{15}O_2$–$C^{15}O_2$ scan (T in Eq. 6), and the $C^{15}O$ radioactivity against the $^{15}O_2$ radioactivity (A_{co} in Eq. 6). The time lags selected were 60, 100, 200, 400, and 800 s, and the inhaled $C^{15}O$ radioactivity was either 25% (case '25%') or 100% (case '100%') of the $^{15}O_2$ inhaled radioactivity. 100 sets of noisy arterial TACs for $C^{15}O$ were realized by assuming that the standard deviation of the $C^{15}O$ radioactivity was equal to the square root of the $C^{15}O$ radioactivity. Figure 2 (left) shows the CIF after $^{15}O_2$ gas inhalation in a case where the time lag was 60 s. These TACs did not correct the physiological decay of $^{15}O_2$. For the subtraction method, $A_{True}(t)$ in Eq. 8 was computed for each dataset.

Simulated tissue TAC with CO radioactivity

Using the typical input function and Eq. 1, the tissue TAC during a $^{15}O_2$–$C^{15}O_2$ scan was simulated. We considered two physiological conditions, namely the normal condition

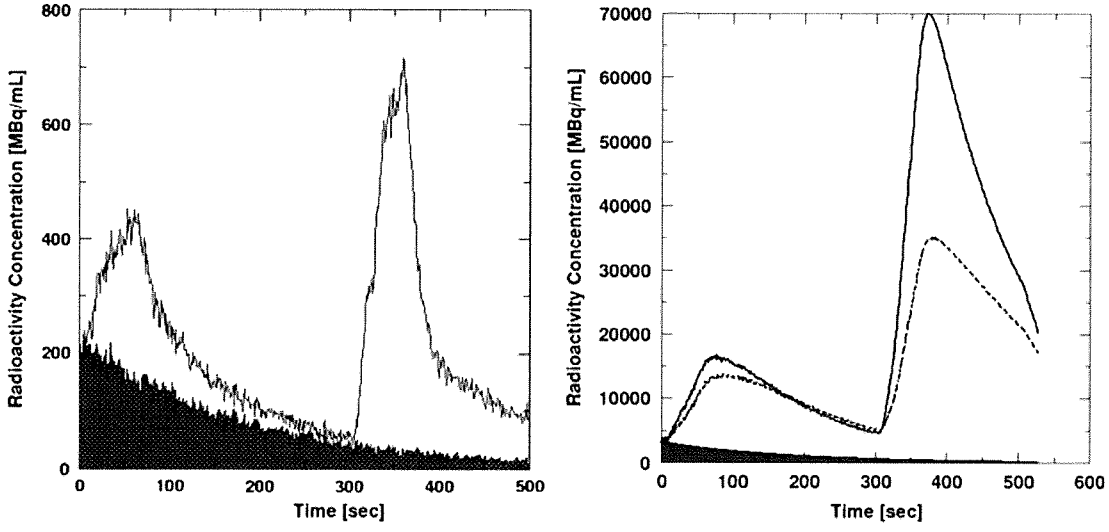

Fig. 2 Input function (*left*) and PET count curves (*right*) during the $^{15}O_2$–$C^{15}O_2$ scan. These curves have the added residual $C^{15}O$ radioactivity (hatched region). The interval time for the $C^{15}O$ and $^{15}O_2$ is 60 s, and the inhaled $C^{15}O$ radioactivity is 100% of the peak value for $^{15}O_2$. $C^{15}O$ time-activity curve. The *solid line* in the *right graph* indicates the PET counts in the normal model, and the *dashed line* is the PET counts in the ischemic model

(CBF = 0.5 mL/g tissue/min, OEF = 0.4, CBV = 0.04, mL/g, p = 0.8 mL/g, Fv = 0.835, and R_{Hct} = 0.85) and an ischemic condition (CBF = 0.2 mL/g tissue/min, OEF = 0.7, CBV = 0.04 mL/g, p = 0.8 mL/g, Fv = 0.835, and R_{Hct} = 0.85). The tissue radioactivity from the residual $C^{15}O$ radioactivity was added to the simulated tissue TACs using Eq. 7. 100 sets of noisy tissue TACs were generated using an NEC model [19]. Figure 2 (right) shows a simulated tissue TAC under the condition of a time lag of 60 s and the case '100%'. For the subtraction method, $C_{True}(t)$ in Eq. 9 was computed for each dataset.

Calculation and evaluation of CBF and OEF values

The $H_2^{15}O$ contents (A_{H_2O}) and $^{15}O_2$ contents (A_{O_2}) were separated from the input functions using the separation method proposed by Kudomi et al. [16]. This separation is demonstrated in Fig. 3. The CBF and OEF values were computed from the A_{H_2O}, A_{O_2}, and the tissue TACs by means of Eqs. 4 and 5. The errors, in the form of bias and coefficient of variance (COV), in the estimated CBF and OEF values were calculated by comparing them with the true CBF and OEF values.

Results

Tables 1 and 2 show the results of the estimated values and COV for CBF and OEF in this simulation study using the conventional DARG method in the cases of the normal model and ischemic model, respectively. As shown in these tables, the estimated CBF and OEF values were underestimated in all cases due to the residual $C^{15}O$ radioactivity. For instance, in the case of the normal model and a time lag of 60 s, the underestimation of the estimated OEF value

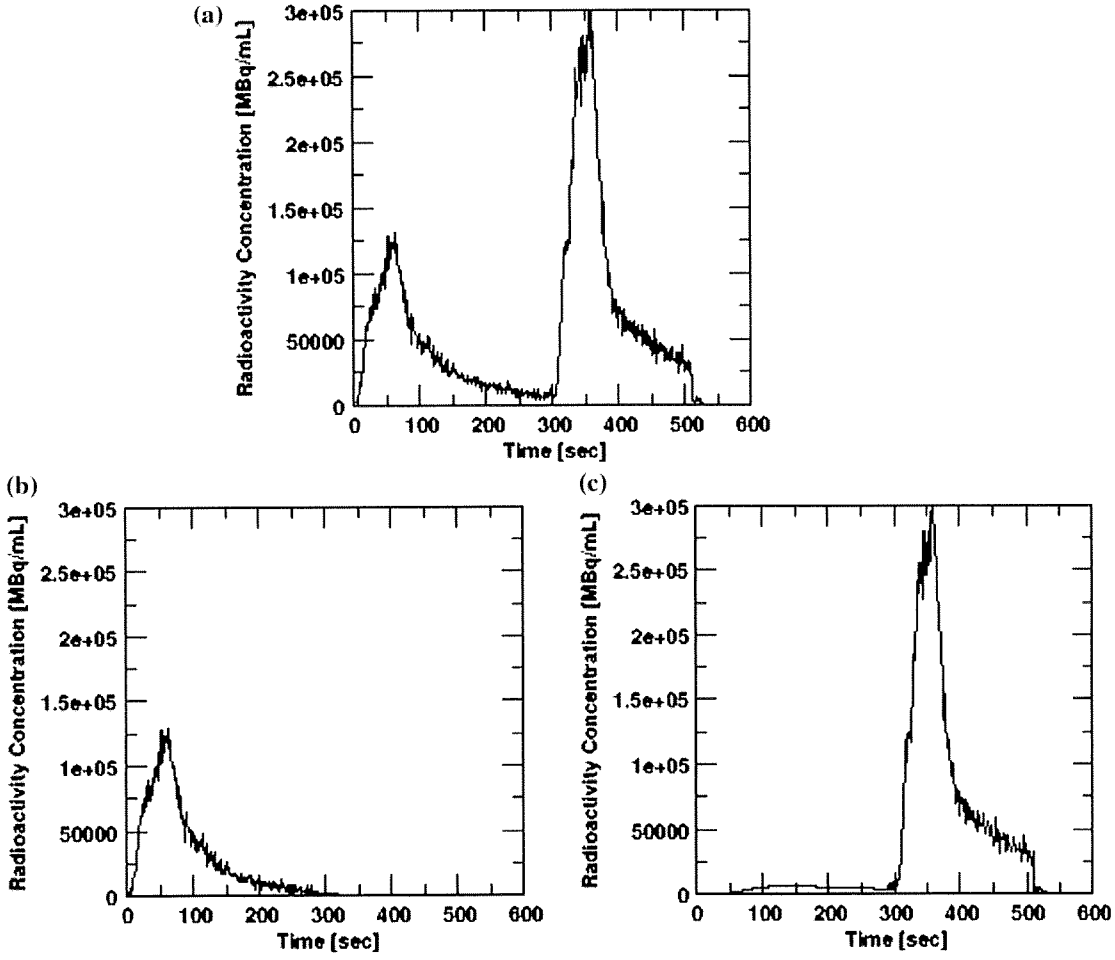

Fig. 3 Separation of the input function for the $^{15}O_2$–$C^{15}O_2$ scan. Total input function (**a**), $^{15}O_2$ input function (**b**), and $C^{15}O_2$ input function (**c**) separated from the total input function. The radioactivity observed earlier than 300 s in the graph (**c**) is the recirculation water

Table 1 Summary of simulation for CBF and OEF in the case '25%' and the case '100%' of the normal model using the conventional DARG method

$C^{15}O$–$^{15}O_2$ time lag (s)	CBF			OEF		
	Average (mL/g/min)	Error (%)	COV (%)	Average	Error (%)	COV (%)
Case '25%'						
60	0.49	−2.06	1.07	0.30	−25.0	1.06
100	0.49	−1.82	0.66	0.31	−21.0	0.52
200	0.50	−0.12	0.23	0.35	−13.5	0.33
400	0.50	−0.04	0.17	0.38	−4.55	0.19
800	0.50	−0.02	0.06	0.40	−0.48	0.07
Case '100%'						
60	0.46	−7.55	1.68	0.16	−60.9	1.64
100	0.47	−6.05	1.37	0.18	−54.4	1.25
200	0.48	−3.91	0.92	0.25	−38.7	0.823
400	0.49	−1.51	0.42	0.34	−16.0	0.45
800	0.50	−0.19	0.08	0.39	−1.90	0.12

Table 2 Summary of simulation for CBF and OEF in the case '25%' and the case '100%' of ischemic model using the conventional DARG method

$C^{15}O$–$^{15}O_2$ time lag (s)	CBF			OEF		
	Average (mL/g/min)	Error (%)	COV (%)	Average	Error (%)	COV (%)
Case '25%'						
60	0.20	−2.72	0.30	0.55	−21.3	0.48
100	0.20	−2.18	0.26	0.58	−17.8	0.37
200	0.20	−1.30	0.17	0.62	−10.9	0.30
400	0.20	−0.45	0.07	0.67	−3.83	0.16
800	0.20	−0.04	0.02	0.70	−0.39	0.06
Case '100%'						
60	0.18	−8.27	0.88	0.33	−52.6	1.08
100	0.19	−6.84	0.71	0.37	−46.9	0.85
200	0.19	−4.43	0.43	0.47	−33.1	0.62
400	0.20	−1.70	0.18	0.61	−13.6	0.36
800	0.20	−0.20	0.04	0.69	−1.60	0.11

was −25% for the case '25%' and −61% for the case '100%'. Larger underestimation values were observed for shorter time lags. The OEF estimation was more sensitive to the residual CO radioactivity than the CBF estimation. Less underestimation was observed in the CBF value in the normal model than in the ischemic model. On the other hand, a larger underestimation was observed in the OEF value in the normal model compared to the ischemic model. The COV was always larger in the normal model than in the ischemic model.

Tables 3 and 4 show the results of the estimated values and the COV for CBF and OEF using the subtraction method. As shown in the tables, no underestimation was observed in all cases. Moreover, the COV values were less than one by the conventional method.

Discussion

CBV images are widely used for the diagnosis of cerebrovascular disease [20]. These images are also utilized to correct the vascular space in the DARG method for CBF and OEF values [15]. Therefore, a $C^{15}O$ scan is mandatory for the DARG protocol. Due to a desire to shorten the total study period, it is often observed that the $^{15}O_2$–$C^{15}O_2$ scan is initiated without waiting long enough for the physical decay of the $C^{15}O$ radioactivity. In this paper, the influences of this residual $C^{15}O$ radioactivity on the CBF and OEF values for the DARG protocol were evaluated by means of computer simulations. According to the results, the CBF and OEF values were underestimated because of the residual $C^{15}O$ radioactivity. The magnitude of the

Table 3 Summary of simulation for CBF and OEF in the case '25%' and the case '100%' of normal model using the DARG method with the subtraction method

$CO–O_2$ time lag (s)	CBF			OEF		
	Average (mL/g/min)	Error (%)	COV (%)	Average	Error (%)	COV (%)
Case '25%'						
60	0.50	0.15	0.37	0.40	−0.17	0.54
100	0.50	0.16	0.33	0.40	−0.18	0.41
200	0.50	0.08	0.27	0.40	−0.31	0.34
400	0.50	−0.04	0.13	0.40	−0.60	0.18
800	0.50	0.02	0.04	0.40	0.12	0.07
Case '100%'						
60	0.50	0.28	0.53	0.40	−0.24	1.02
100	0.50	0.32	0.53	0.40	−0.45	0.97
200	0.50	0.17	0.40	0.40	−0.61	0.70
400	0.50	0.04	0.27	0.40	−0.34	0.41
800	0.50	−0.02	0.07	0.40	−0.17	0.12

Table 4 Summary of simulation for CBF and OEF in the case '25%' and the case '100%' of ischemic model using the DARG method with the subtraction method

$CO–O_2$ time lag (s)	CBF			OEF		
	Average (mL/g/min)	Error (%)	COV (%)	Average	Error (%)	COV (%)
Case '25%'						
60	0.20	0.05	0.15	0.70	−0.13	0.46
100	0.20	0.05	0.14	0.70	−0.14	0.36
200	0.20	0.00	0.11	0.70	−0.25	0.29
400	0.20	−0.05	0.06	0.70	−0.51	0.16
800	0.20	0.01	0.02	0.70	0.11	0.06
Case '100%'						
60	0.20	0.09	0.25	0.70	−0.22	0.86
100	0.20	0.10	0.24	0.70	−0.36	0.83
200	0.20	0.03	0.17	0.70	−0.50	0.62
400	0.20	−0.01	0.11	0.70	−0.27	0.36
800	0.20	−0.02	0.04	0.70	−0.15	0.11

underestimation depended on the amount of $C^{15}O$ radioactivity, the time interval between the $C^{15}O$ scan and the $^{15}O_2$–$C^{15}O_2$ scan, and the disease model we assumed. By subtracting the $C^{15}O$ radioactivity from the input function and PET counts, this underestimation could be eliminated, which resulted in shortening the total study period of the DARG protocol.

Underestimation of CBF and OEF values due to residual $C^{15}O$ radioactivity

In general, overestimations of the arterial radioactivity or PET counts can cause underestimation or overestimation of physiological measures (CBF and OEF), respectively, in the DARG method. Thus, the residual $C^{15}O$ radioactivity might induce the bias in either of direction. As shown in our results, the estimated CBF and OEF values were both underestimated due to the residual $C^{15}O$ radioactivity, which indicates that the bias of the input function by the $C^{15}O$ radioactivity more strongly influenced the estimates than the bias of the PET counts by the $C^{15}O$ radioactivity. In our simulation, the CBV was fixed as 0.04 mL/mL. If the larger CBV was assumed (i.e. dilatation of blood vessel), more residual $C^{15}O$ radioactivity was added on the PET counts and the bias of the total PET counts was increased by Eq. 1, which results in less underestimation for the CBF and OEF values. Note that in this paper, we evaluated not $CMRO_2$ but OEF. $CMRO_2$ is derived by being multiplied CBF and OEF values. Thus, the magnitude of the underestimation in $CMRO_2$ could be larger than those of CBF and OEF.

Tables 1 and 2 suggest that the normal model underestimated OEF more than the ischemic model because of the residual $C^{15}O$ radioactivity. On other hand, the normal

model underestimated CBF less than the ischemic model because of the residual $C^{15}O$ radioactivity. Although the DARG method uses $^{15}O_2$ phase (PET data before the inhalation of $C^{15}O_2$) and $C^{15}O_2$ phase (PET data after the inhalation of $C^{15}O_2$) datasets, and simultaneously estimates CBF and OEF values, the PET data of the $^{15}O_2$ phase were dominant in the determination of OEF and those of the $C^{15}O_2$ phase were dominant in the determination of CBF. As shown in Tables 1 and 2, the amount of the underestimation for OEF is larger than for CBF, which can be explained by the amount of residual $C^{15}O$ radioactivity in both phases. As shown in Fig. 2, the influence of $C^{15}O$ on the input function was much higher in the $^{15}O_2$ phase than in the $C^{15}O_2$ phase. The residual $C^{15}O$ radioactivity led to the underestimation of CBF, mainly determined in the $C^{15}O_2$ phase. However, this underestimation was not enough to explain the bias of the input function in the $^{15}O_2$ phase. The first term on the right side of Eq. 1 has only CBF (f) as a parameter and the value of the first term is much higher in the normal model than in the ischemic model due to the higher CBF of the normal model, which implies that a greater underestimation for OEF could occur in the normal model to compensate for the insufficient underestimation of CBF. The ischemic model has a lower CBF than the normal model, which results in the slow washout of $^{15}O_2$ in tissue (the second term on the right side of Eq. 1). Therefore, the ischemic model has a greater source of underestimation for CBF than the normal model during the $C^{15}O_2$ phase.

As shown in Tables 1, 2, 3, and 4, the COVs of CBF and OEF in the ischemic model were smaller than the COVs in the normal model. The non-linear relationship between the PET counts and CBF attributed to this phenomenon [13]. The PET counts of the normal model were higher than those of the ischemic model, and the higher PET counts emphasized the noise due to this non-linearity.

Our results suggest that attention must be paid to the interpretation of CBF and OEF images from DARG, if contaminated by the significant amount of the residual $C^{15}O$ radioactivity namely: the magnitude of the error may not be uniform across different physiological conditions in the brain.

Subtraction method

The subtraction method successfully eliminated the influence of the $C^{15}O$ radioactivity on both the input function and PET counts during the $^{15}O_2$–$C^{15}O_2$ scan, and no errors in the CBF and OEF values due to the residual $C^{15}O$ radioactivity were observed. In theory, there is no statistical advantage for the subtraction method compared to the conventional method. However, as shown in Tables 3 and 4, the COV by the subtraction method was smaller than the value by the conventional method. It is necessary to separate the $^{15}O_2$ contents and $C^{15}O_2$ contents in the measured input function prior to the DARG calculation. For this separation, we utilized the linear method proposed by Kudomi et al. [16]. The linear method estimates the $^{15}O_2$ contents in the input function after $C^{15}O_2$ inhalation by linear extrapolation. In the conventional method, due to the offset of the input function by the residual $C^{15}O$ radioactivity, the estimated $^{15}O_2$ contents remain until the last in most cases. On other hand, in the subtraction method, by subtracting the $C^{15}O$ radioactivity from the input function, the offset of the input function is removed. Then, in many cases the $^{15}O_2$ contents estimated by the extrapolated line go to zero. This causes a reduction of the variation in the estimated CBF and OEF values compared to the conventional method.

The estimation of the recirculation water in the input function is based on the empirical model [10], and this model may not work owing to the residual $C^{15}O$ radioactivity, which results in biased CBF and OEF values. This bias can be removed by the subtraction method. Thus, by using the subtraction method, accurate CBF and OEF values can be measured no matter how much $C^{15}O$ radioactivity exists, which results in shortening the total PET study. The subtraction method could be applied, not only to the DARG protocol, but also to the conventional ARG and steady-state protocols. In this simulation, we assumed no biological decay of $C^{15}O$, which is not true in the actual data, and the subtraction method might over-subtract the influence of $C^{15}O$ radioactivity. The biological half-life of $C^{15}O$ is difficult to determine within a period of ordinary PET scan owing to the short life of the ^{15}O radionuclide. We tested simulated data with a biological half-life of 10 min, and there were no significant differences in the estimated CBF and OEF values compared to the results shown in this paper. In order to apply the subtraction method in clinical study, further studies are, however, required to verify the influence of biological decay.

Sequence of PET scans

In this paper, the sequence of the scans was a $C^{15}O$ scan followed by a $^{15}O_2$–$C^{15}O_2$ scan. If the $C^{15}O$ scan was performed after the $^{15}O_2$–$C^{15}O_2$ scan, our results were not valid. The reason for this sequence ($C^{15}O$ scan followed by a $^{15}O_2$–$C^{15}O_2$ scan) was to shorten the total duration of the PET study by exchanging the target gas (from N_2 containing O_2 to N_2 containing CO_2) only once (the synthesis of $C^{15}O$ and $^{15}O_2$ shares the same target in a cyclotron but uses different one from that of $C^{15}O_2$). Furthermore, the sequence of $^{15}O_2$–$C^{15}O_2$ produces better results than the sequence of $C^{15}O_2$–$^{15}O_2$ [15]. In order to further shorten the total study time, more development efforts are needed

in relation to the delivery system for the radioactive gases, which should have the ability to deliver such gases quickly.

The results in this paper were based only on the computer simulations. It could be expected to have several difficulties to show validities of our results using actual PET measurements by several reasons such as (1) PET cannot differentiate between photon from residual $C^{15}O$ and photon from either $^{15}O_2$ or $C^{15}O_2$, (2) large inter-subject variation for cerebrovascular disease, (3) large amounts of radiation exposure to patients from $C^{15}O$ in the case of large inhalation of $C^{15}O$. For the validation of our results, PET studies with ischemic animal model will be anticipated.

Conclusions

In this paper, we verified the influence of $C^{15}O$ radioactivity on the computation of CBF and OEF using the DARG protocol. We found that the bias and noise in the CBF and OEF values depended on the amount of residual $C^{15}O$ radioactivity during the scanning for $^{15}O_2$ and $C^{15}O_2$, and on the physiological conditions of the brain tissue. By using the subtraction method, the bias could be eliminated. Finally, we discussed the effects of the recirculation water and the biological decay for $C^{15}O$ radioactivity on the computation of CBF and OEF using the DARG method.

References

1. Frackowiak RS, Jones T, Lenzi GL, Heather JD. Regional cerebral oxygen utilization and blood flow in normal man using oxygen-15 and positron emission tomography. Acta Neurol Scand. 1980;62:336–44.
2. Frackowiak RS, Lenzi GL, Jones T, Heather JD. Quantitative measurement of regional cerebral blood flow and oxygen metabolism in man using 15O and positron emission tomography: theory, procedure, and normal values. J Comput Assist Tomogr. 1980;4:727–36.
3. Mintun MA, Raichle ME, Martin WR, Herscovitch P. Brain oxygen utilization measured with O-15 radiotracers and positron emission tomography. J Nucl Med. 1984;25(2):177–87.
4. Lammertsma AA, Jones T. Correction for the presence of intravascular oxygen-15 in the steady-state technique for measuring regional oxygen extraction ratio in the brain: 1. Description of the method. J Cereb Blood Flow Metab. 1983;3:416–24.
5. Subramanyam R, Alpert NM, Hoop B Jr, Brownell GL, Yaveras JM. A model for regional cerebral oxygen distribution during continuous inhalation of 15O2, C15O, and C15O2. J Nucl Med. 1978;19:48–53.
6. Lammertsma AA, Heather JD, Jones T, Frackowiak RS, Lenzi GL. A statistical study of the steady state technique for measuring regional cerebral blood flow and oxygen utilization using 15O. J Comput Assist Tomog. 1982;6:566–73.
7. Correia JA, Alpert NM, Buxton RB, Ackerman RH. Analysis of some errors in the measurement of oxygen extraction and oxygen consumption by the equilibrium inhalation method. J Cereb Blood Metab. 1985;5:591–9.
8. Okazawa H, Ymauchi H, Sugimoto K, Takahashi M, Toyoda H, Kishibe Y, et al. Quantitative comparison of the bolus and steady-state methods for measurement of cerebral perfusion and oxygen metabolism: positron emission tomography study using 15O-gas and water. J Cereb Blood Metab. 2001;21:793–803.
9. Okazawa H, Ymauchi H, Sugimoto K, Toyoda H, Kishibe Y, Takahashi M. Effects of acetazolamide on cerebral blood flow, blood volume, and oxygen metabolism: a positron emission tomography study with healthy volunteers. J Cereb Blood Flow Metab. 2001;21:1472–9.
10. Iida H, Jones T, Miura S. Modeling approach to eliminate the need to separate arterial plasma in oxygen-15 inhalation positron emission tomography. J Nucl Med. 1993;34:1333–40.
11. Sadato N, Yonekura Y, Senda M, Iwasaki Y, Matoba N, Tamaki N, et al. PET and the autoradiographic method with continuous inhalation of oxygen-15-gas: theoretical analysis and comparison with conventional steady-state methods. J Nucl Med. 1993; 34:1672–80.
12. Hatazawa J, Fujita H, Kanno I, Satoh T, Iida H, Miura S, et al. Regional cerebral blood flow, blood volume, oxygen extraction fraction, and oxygen utilization rate in normal volunteers measured by the autoradiographic technique and the single breath inhalation method. Ann Nucl Med. 1995;9:15–21.
13. Shidahara M, Watabe H, Kim KM, Oka H, Sago M, Hayashi T, et al. Evaluation of a commercial PET tomograph-based system for the quantitative assessment of rCBF, rOEF and rCMRO2 by using sequential administration of ^{15}O-labeled compounds. Ann Nucl Med. 2002;16(5):317–27.
14. Hattori N, Bergsneider M, Wu HM, Glenn TC, Vespa PM, Hovda DA, et al. Accuracy of a method using short inhalation of 15O–O2 for measuring cerebral oxygen extraction fraction with PET in healthy humans. J Nucl Med. 2004;45:765–70.
15. Kudomi N, Hayashi T, Teramoto N, Watabe H, Kawachi N, Ohta Y, et al. Rapid quantitative measurement of $CMRO_2$ and CBF by dual administration ^{15}O-labeled oxygen and water during a single PET scan—a validation study and error analysis in anesthetized monkeys. J Cereb Blood Flow Metab. 2005;25:1209–24.
16. Kudomi N, Watabe H, Hayashi T, Iida H. Separation of input function for rapid measurement of quantitative $CMRO_2$ and CBF in a single PET scan with a dual tracer administration method. Phys Med Biol. 2007;52(7):1893–908.
17. Kudomi N, Choi E, Yamamoto S, Watabe H, Kim KM, Shidahara M, et al. Development of a GSO Detector Assembly for a Continuous Blood Sampling System. IEEE Trans Nucl Sci. 2003; 50(1):70–3.
18. Carson RE. Parameter estimation in positron emission tomography. In: Phelps ME, Mazziotta JC, Schelbert HR, editors. Positron emission tomography and autoradiography. New York: Raven Press; 1986. p. 347–90.
19. Shidahra M, Watabe H, Kim KM, Kudomi N, Ito H, Iida H. Optimal scan time of oxygen-15-labeled gas inhalation autoradiographic method for measurement of cerebral oxygen extraction fraction and cerebral oxygen metabolic rate. Ann Nucl Med. 2008;22(8):667–75.
20. Ito H, Kanno I, Fukuda H. Human cerebral circulation: positron emission tomography studies. Ann Nucl Med. 2005;19(2):65–74.


３．PET 装置ならびに関連技術の進歩

国立循環器病センター研究所　先進医工学センター　放射線医学部
越野一博　平野祥之　寺本昇　渡部浩司　飯田秀博

１．はじめに

PET (positron emission tomography)は、SPECT と並ぶ核医学的診断手法の一つで、陽電子放出核種を用いて断層撮像を行い、病態の変化や治療効果を高感度、低侵襲で観察することが可能である。PET では多種多様な放射性薬剤（トレーサー）を用いることで、トレーサーの体内における分布や動態から、血流量、酸素代謝率や酸素摂取率などの循環代謝、脂肪酸、ブドウ糖やアミノ酸に代表される基質代謝および神経伝達・受容体機能を画像化・定量評価することが可能である。本稿では、PET 装置および関連技術の進歩、そして心筋 PET の有用性と課題について紹介する。

２．PET 装置の進歩

PET 装置の基本性能の主な指標として、空間分解能、感度、最高係数率がある。トレーサー核種から放出された陽電子が体内組織の電子と対消滅を起こすと、一対のγ線が発生する。γ線を精度良く検出することは、高解像度の PET 画像が得られることにつながり、例えば FDG-PET においては、腫瘍と正常組織との判別を容易にし、診断能の向上につながる。またγ線を高感度で検出することは、少量のトレーサーによる画像診断を可能とし、被検者の被ばく低減につながる。優れた最高係数率の装置では、γ線の数え落としが少なく、偶発・散乱同時計数の影響を受けにくいため、定量精度を保証する要因となる。本節では、PET の原型となる装置(PETT)が 1975 年に Ter-Pogossian らによって発表されて以降、高空間分解能や高感度撮像を実現するために開発されてきた装置および技術について述べる[1-2]。

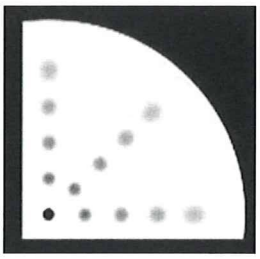

図１　辺縁部での画質低下
（シーメンス旭メディテック（株）提供）

２．１ 撮像装置

従来型 PET ではγ線検出器の厚みにより、視野辺縁部では感度分布が広がり空間分解能が低下するという問題があった（図 1)。この様な問題を解決するために DOI-PET（depth-of-interaction PET）や TOF- PET

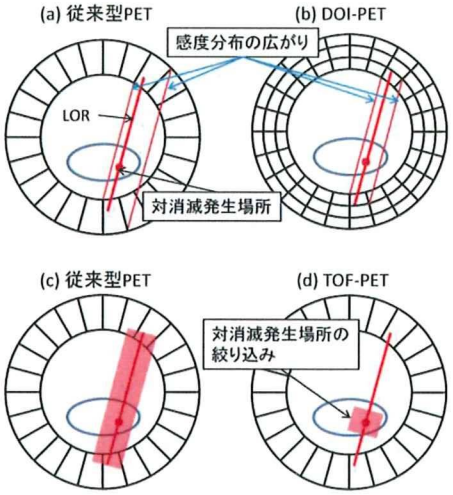

図２　従来型 PET 装置と DOI-PET および TOF-PET の概念図

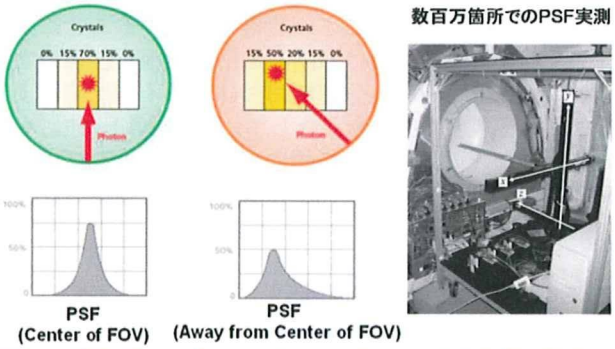

図３　PSF（Point Spread Function）による入射角の推定
（シーメンス旭メディテック（株）提供）

(time-of-flight PET)が開発されている。図２に従来型 PET と DOI-PET および TOF-PET の概念図を示した。DOI-PET では、検出器における深さ方向の相互作用位置を利用することで、感度分布の広がりを抑制し、空間分解能および感度を向上させた。PET 装置で測定される情報は電子－陽電子対消滅により発生したγ線の発生場所ではなく、一対のγ線検出器を結ぶ LOR (line-of-response)である。TOF-PET は二個の検出器にγ線が到達する時間差を利用して、LOR 上のγ線発生場所を測定し、空間分解能および感度の向上を実現している。

２．２ 画像再構成

装置の性能向上に加えて、新しい画像再構成法も提

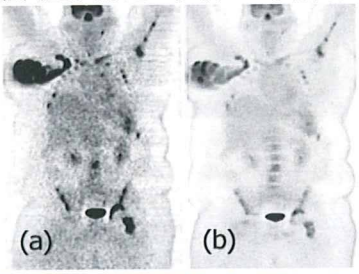

図4 HD・PETによる画像再構成 (a) PSFなし (b) PSFあり
（シーメンス旭メディテック（株）提供）

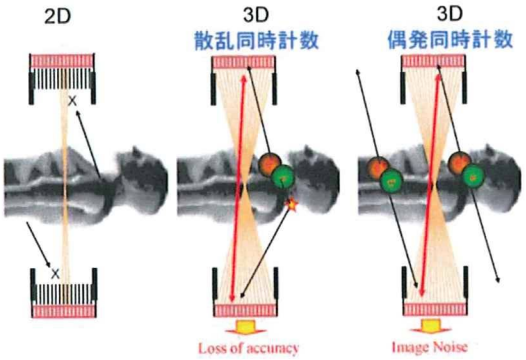

図5 2D-PETおよび3D-PETにおけるノイズの影響

案されている。その1例として、点広がり関数（PSF、point-spread-function）を用いた画像再構成法がある。図3のようにあらかじめ視野内における点広がり関数を測定し、画像再構成時にこの情報を利用することによって、視野辺縁部における画質劣化を抑制し、視野内全域における均一な高分解能および、ノイズ低減によるコントラストの向上を果たしている（図4）。他にもMRI画像などの形態情報を用いて画像再構成を行い、PET画像の空間分解能を向上させる手法も提案されている。

2．3 2D-PETおよび3D-PET

2D-PET装置は、リング間に散乱線を除去するためのセプタ構造をもち、定量性が高い反面、感度が低い。現在主流となっている3D-PETはセプタをもたず、多層のリング間での同時計数を測定するため、感度が2D収集時に比べて6～8倍高い。PET-CT装置はほとんどが3D-PETである。感度が高い一方で、散乱線などが増加するため、定量性は2D-PETに比べて劣るといわれてきた（図5）。しかしながら3D-PETを用いた^{13}N-アンモニアや^{15}O-標識水 心筋PET検査における定量性について評価が進んでいる[3-4]。

3．心筋PETイメージング

3．1 心筋PET検査の有用性

心臓イメージングにおいては、CT angiography (CTA)を用いた冠動脈病変に関する報告が多数なされている。しかしながらCTAでは、高輝度信号として観測される石灰化プラークなどにおいて、その信号が本来の大きさを超えて近傍領域に広がって観測されるため、狭窄

重症度を過大評価することや、CTAによる形態情報に

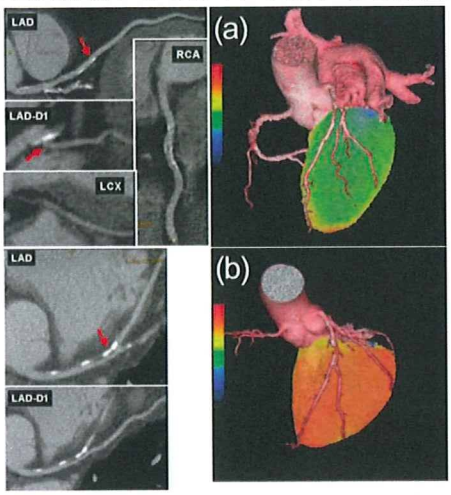

図6 動脈硬化症例における血管反応性の画像評価。CT angiographyによる血管形態画像と^{15}O-標識水PETによる心筋灌流画像の融合。共に狭窄が認められるが、(a) 血流予備能が低下している例 (b) 血管予備能が保たれている例（Finland, Truku PETセンター Knuuti教授提供）

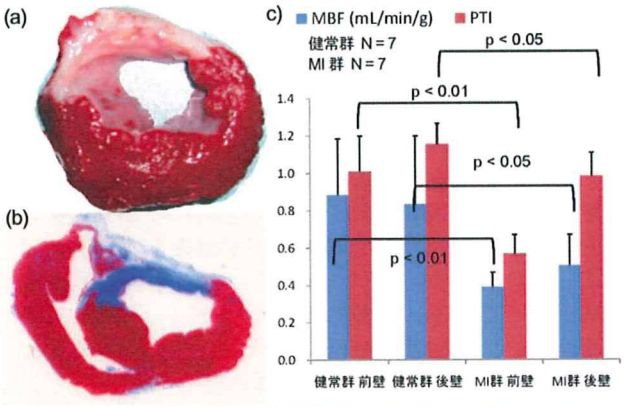

図7 家畜ブタを対象とした^{15}O-標識水PET (a) Macro (b) Histology (c) 心筋血流量 (MBF) とPTI値に関する比較

基づく予測と、PETやSPECTなど生理学的情報による心筋虚血診断との乖離が指摘されている[5]。Knuutiらは、CTモダリティの高空間分解能という利点を生かした血管形態画像と、^{15}O-標識水PETによる心筋灌流画像を図6のように三次元的に融合し、その有用性を報告している[6]。図6は、CTAでは共に狭窄を有する症例であるが、^{15}O-標識水PETによって得られた心筋血流予備能が顕著に異なっている例である。心筋虚血の指標の一つである血流予備能には、狭窄以外の微少循環に関わる因子が関与していると考えられている。循環器病疾患の予防や治療の客観的評価を可能とする微小血管の機能と構築に関する診断法の確立が期待されている。^{15}O-標識水PETでは、心筋血流量や血流予備能の他に、灌流可能な心筋組織すなわち微小循環に関する評価が可能である。

我々のグループが家畜ブタ心筋梗塞モデルを対象に行った^{15}O-標識水PET実験では、病態モデル群において心拍数、駆出率、拡張期圧について健常群に対する有意な低下が認められた。PET解析では、梗塞（前壁）

領域だけでなく、対側（後壁）領域においても組織血流量（MBF）と灌流可能な心筋組織の割合（PTI）の有意な低下が認められた（図7）。病理組織学的所見では、対側領域の心壁肥厚の他、心筋組織の線維化が観察された。対側領域における PTI の低下は、そのような現象を反映していると考えている。PTI に関しては、値 0.7 をカットオフとする、viable と non-viable な組織の判別の可能性が示唆されている[7-9]。現在、我々のグループでは、家畜ブタおよびミニブタ心筋梗塞モデルを対象とした心筋シート移植再生医療において、PTI のサロゲートマーカーとしての有用性を検証中である。

PET との一体型装置として、PET-MRI 装置の開発も進んでいる[1)、10)]。MRI は CT よりも軟組織の描出に優れており、詳細な形態情報に基づく心機能（拍出量、駆出率、心壁厚変化など）や冠動脈狭窄評価に適したモダリティである。一体型 PET-MRI 装置では、PET-CT 装置と比較しての被ばく量低減、PET および MRI の同時撮像による検査時間の短縮化に加えて、生理学的機能評価と形態・運動機能評価の融合による循環器病疾患の本態解明が進むと期待されている。

3．2 心筋イメージングの課題

PET は、1) SPECT と比較して 100 倍以上の高い感度、2) 高空間分解能、3) 虚血診断およびバイアビリティに対する高い診断精度（感度・特異度）、3) 多様なトレーサーが利用可能、という特徴を有し、心筋イメージングにおける優れたモダリティの一つである。しかしながら、全国の PET 装置普及台数は SPECT 装置の 1/10 以下である。PET 装置の普及を妨げている要因としては、装置自体のコストの他に、トレーサー合成や定量精度において、1) 施設外供給可能なトレーサーが ^{18}F-FDG のみ、2) その他のトレーサーに関しては、短い放射性半減期を原因とする院内サイクロトロンの設置、あるいはジェネレーターの製造および供給体制の整備、3) 3D-PET または PET-CT 装置における定量性の検証、4) 定量解析手法の標準化、という問題や課題がある。本稿で紹介した ^{15}O 標識水心筋 PET は、正確な血流定量が可能であるが、上述した課題が残されている。心筋 PET が普及する必要条件として、トレーサー合成の観点からは、高い extraction fraction および残存細胞に依存した再分布を備えた ^{18}F 標識トレーサーあるいは ^{15}O 標識ガス超小型・全自動検査システムの開発が望まれる。定量化の観点からは、3D-PET における定量精度の確保、定量解析手法の標準化などがある。これらの課題を克服することで、心筋 PET イメージングの有用性はさらに高まると思われる。

4．おわりに

本稿では、PET 装置および関連技術の進歩、そして心筋 PET の有用性と課題について紹介した。心筋 PET イメージングは病態把握、医薬品の安全性・薬効評価や再生医療への応用など、今後も重要な役割を果たすと考える。

参考文献

1) Pichler BJ et al: J Nucl Med **49** : Suppl 2:5-23, 2008
2) Lecomte R: Eur J Nucl Med Mol Imaging. **36** Suppl 1:S69-85, 2009
3) Schepis T et al: J Nucl Med **48** : 783-789, 2007
4) Roelants V et al: J Nucl Cardiol **13**: 220-224, 2006
5) Di Carli MF et al: Circulation **115**:1464-1480, 2007
6) Knuuti J et al: Heart **94**:360-367, 2008
7) Yamamoto Y et al: Circulation **86**:167-178, 1992
8) de Silva R et al: Circulation **86**:1738-1742, 1992
9) Knappen et al: J Nucl Med **45**: 1299-304, 2004
10) Wehrl HF et al: Eur J Nucl Med Mol Imaging **36** Suppl 1: S56-68, 2009

NeuroImage xxx (2009) xxx–xxx

Contents lists available at ScienceDirect

NeuroImage

journal homepage: www.elsevier.com/locate/ynimg

Quantitative evaluation of changes in binding potential with a simplified reference tissue model and multiple injections of [^{11}C]raclopride

Yoko Ikoma [a,b,*], Hiroshi Watabe [a], Takuya Hayashi [a], Yoshinori Miyake [c], Noboru Teramoto [a], Kotaro Minato [b], Hidehiro Iida [a]

[a] Department of Investigative Radiology, National Cardiovascular Center Research Institute, Suita, Osaka, Japan
[b] Graduate School of Information Science, Nara Institute of Science and Technology, Ikoma, Nara, Japan
[c] Department of Radiology and Nuclear Medicine, National Cardiovascular Center Hospital, Suita, Osaka, Japan

ARTICLE INFO

Article history:
Received 20 February 2009
Revised 27 May 2009
Accepted 29 May 2009
Available online xxxx

Keywords:
Positron emission tomography
[^{11}C]raclopride
Dopamine D_2 receptor
Multiple injections
Binding potential

ABSTRACT

Positron emission tomography (PET) with [^{11}C]raclopride is widely used to investigate temporal changes in the dopamine D_2 receptor system attributed to the dopamine release. The simplified reference tissue model (SRTM) can be used to determine the binding potential (BP_{ND}) value using the time–activity curve (TAC) of the reference region as input function. However, in assessing temporal changes in BP_{ND} using the SRTM, multiple [^{11}C]raclopride PET scans are required, and a second scan must be performed after the disappearance of the [^{11}C]raclopride administered in the first scan. In this study, we have developed an extended multiple-injection SRTM to estimate the BP_{ND} change, from a single PET scan with multiple injections of [^{11}C]raclopride, and we have validated this approach by performing numerous simulations and studies on monkeys. In the computer simulations, TACs were generated for dual injections of [^{11}C]raclopride, in which binding conditions changed during the scans, and the BP_{ND} values before, and after, the second injection were estimated by the proposed method. As a result, the reduction in BP_{ND} was correlated, either with the integral of released dopamine, or with the administered mass of raclopride. This method was applied to studies on monkeys, and was capable of determining two identical BP_{ND} values when there were no changes in binding conditions. The BP_{ND} after the second injection decreased when binding conditions changed due to an increase in administered raclopride. An advantage of the proposed method is the shortened scan period for the quantitative assessment of the BP_{ND} change for neurotransmitter competition studies.

Introduction

Neuroreceptor imaging using positron emission tomography (PET) and [^{11}C]raclopride has made it possible to determine the density of striatal dopamine D_2 receptors *in vivo* (Farde et al., 1985; Köhler et al., 1985; Hall et al., 1988). The binding potential ($BP_{ND} = k_3/k_4$) derived from rate constants in a two-tissue compartment model has been used to quantify the receptor binding (Mintun et al., 1984). Endres et al. then developed an extended compartment model, which included the released neurotransmitter concentration, and demonstrated that [^{11}C]raclopride binding decreased after the administration of amphetamine, which resulted in the displacement of the raclopride due to competition with increased dopamine (Endres et al., 1997, Carson et al., 1997). The model showed that the change in BP_{ND} between the baseline and the stimulated state was related to the total amount of released dopamine. Applying this theory, it has been shown that amphetamine-related reductions in [^{11}C]raclopride-specific binding in patients with schizophrenia was significantly greater than in healthy volunteers (Breier et al., 1997) and that a reduction in [^{11}C] raclopride binding was observed while playing a video game which resulted in the release of endogenous dopamine (Koepp et al., 1998). In this competition paradigm, two PET studies are necessary to measure the BP_{ND} values of the baseline and competed conditions, and a long study period is required.

On the other hand, single-scan studies with bolus-plus-continuous infusion (B/I) of the tracer, applied for the measurement of reduction in BP_{ND} due to an amphetamine challenge, were also performed (Carson et al., 1997, Endres et al., 1997). In these studies, a stimulus was administered during infusion of the tracer, and the change in binding between pre- and post-amphetamine intervention was measured as the tissue-to-plasma concentration ratio at equilibrium. This method enables the direct measurement of receptor-binding

* Corresponding author. Department of Investigative Radiology, National Cardiovascular Center Research Institute, 5-7-1, Fujishirodai, Suita, Osaka, 565-8565, Japan. Fax: +81 6 6835 5429.
E-mail address: ikoma@ri.ncvc.go.jp (Y. Ikoma).

1053-8119/$ – see front matter © 2009 Elsevier Inc. All rights reserved.
doi:10.1016/j.neuroimage.2009.05.099

changes in a single scan. However, the design of the protocol requires that the tracer kinetics attain equilibrium within the measurement period of the pre- and post-amphetamine challenges (Watabe et al., 2000), and dynamic data that does not reach equilibrium may cause systematic errors in the estimates of binding changes (Zhou et al., 2006).

To compute the BP_{ND} value, the simplified reference tissue model (SRTM) is often used. The SRTM can provide the BP_{ND} without invasive arterial blood sampling by using a time–activity curve (TAC) of the reference region where specific bindings are negligible (Lammertsma and Hume, 1996). Recently, an extended simplified reference tissue model (ESRTM) was developed in order to quantify the reduction in BP_{ND} with B/I administration (Zhou et al., 2006). In the ESRTM method, the BP_{ND} of the SRTM was estimated separately, before and after, the pharmacological challenge during a 90 min scan with B/I administration. The group reported that stimulus-induced BP_{ND} changes, obtained from equilibrium analysis in the non-equilibrium state, resulted in an underestimation of the reduction in BP_{ND}, and that this was significantly improved by using the ESRTM. Nonetheless, B/I administration requires the equipment to provide [^{11}C]raclopride constantly during the scan, and there are often technical problems.

Kim et al. (2006) developed a method to measure regional cerebral blood flow in pre- and post-pharmacological stress from a single session of single photon emission computed tomography (SPECT) scanning with dual injections of ^{123}I-iodoamphetamine. In their paper, they showed mathematical derivation for estimating CBF values from two conditions in a single session of SPECT study. By advancing their method, we have developed a method to detect changes in receptor binding using a single session of PET scanning in conjunction with multiple bolus injections of [^{11}C]raclopride synthesized once before the scan (Watabe et al., 2006). In our approach, the SRTM was extended to measure the BP_{ND} of each injection, and we validated this approach by performing numerous simulations and studies on monkeys using PET and [^{11}C]raclopride.

Methods

Theory

The simplified reference tissue model (SRTM) provides BP_{ND} without arterial blood sampling by eliminating the arterial plasma TAC arithmetically from model equations, by using the TAC of the reference region where specific bindings are negligible. The radioactivity concentration of the target region (C_t) is expressed as Eq. (1), using the radioactivity concentration in the reference region (C_r), under the assumption that the target and reference regions can be expressed using the one-tissue compartment model and that the ratios of K_1 and k_2 are equal between the target and reference regions (Lammertsma and Hume, 1996).

$$C_t(t) = R_1 C_r(t) + \left(k_2 - \frac{R_1 k_2}{1 + BP_{ND}}\right) e^{-\frac{k_2}{1+BP_{ND}}t} \otimes C_r(t) \quad R_1 = K_1 / K_1^r \tag{1}$$

where K_1 and k_2 are the rate constants for the transfer from plasma to the displaceable compartment in the target tissue and from the displaceable compartment to plasma, respectively, and K_1^r is the rate constant for the transfer from plasma to the reference tissue.

We have extended this SRTM to a multiple-injection study. In this approach, the first injection of the radioligand was performed at the time of the scan start, and the BP_{ND} was measured as a baseline. Next, a second injection was performed simultaneously with a change in binding conditions, and the BP_{ND} was measured as a competitive state after the second injection. The BP_{ND} values before, and after, the second injection, were estimated by the multiple-injection simplified reference tissue model (MI-SRTM) expressed as follows:

$$\begin{aligned} C_{t1}(t) &= R_{11} C_{r1}(t) + \left(k_{21} - \frac{R_{11} k_{21}}{1 + BP_{ND1}}\right) e^{-\frac{k_{21}}{1+BP_{ND1}}t} \otimes C_{r1}(t) \\ C_{t2}(t) &= R_{12} C_{r2}(t) + \left(k_{22} - \frac{R_{12} k_{22}}{1 + BP_{ND2}}\right) e^{-\frac{k_{22}}{1+BP_{ND2}}t} \otimes C_{r2}(t) \\ &\quad + (C_{t0} - R_{12} C_{r0}) e^{-\frac{k_{22}}{1+BP_{ND2}}t} \end{aligned} \tag{2}$$

where C_{t1} and C_{t2} are the radioactivity concentrations in the target tissue and C_{r1} and C_{r2} are the radioactivity concentrations in the reference tissue for the first and second injections, respectively; t is the time from the first or second injection; C_{t0} and C_{r0} are the radioactivity concentrations of the target and reference tissues at the time of the second injection, respectively.

Firstly, R_{11}, k_{21} and BP_{ND1} were estimated by nonlinear least squares fitting with the iteration of the Gauss–Newton algorithm using data points before the second injection. Next, C_{r0} was calculated by the interpolation of the measured reference TAC, and C_{t0} was estimated using Eq. (1) with estimated R_{11}, k_{21} and BP_{ND1} values. Finally, R_{12}, k_{22}, and BP_{ND2} were estimated by nonlinear least squares fitting using these C_{r0} and C_{t0} values with Eq. (2). In this study using [^{11}C]raclopride, the TAC of the cerebellum was used as a reference TAC.

The present method can be used to generate voxel-based parametric maps. In the voxel-based estimation for parametric imaging of ligand–receptor binding, R_{11}, k_{21} and BP_{ND1} from the first injection and R_{12}, k_{22}, and BP_{ND2} from the second injection in Eq. (2), were estimated by a basis function method in which the model Eq. (2) is solved using linear least squares for a set of basis functions, which enables the incorporation of parameter bounds (Gunn et al., 1997).

Simulation analysis

Three simulation studies were carried out to validate the present approach and to determine: 1) whether the change in BP_{ND} caused by competition to receptor binding could be detected by the MI-SRTM; 2) how would the time delay between the endogenous dopamine release and [^{11}C]raclopride injection affect BP_{ND} estimates, and 3) what was an optimal scan duration for a reliable BP_{ND} estimation?

Detection of BP_{ND} change with dual injections

The MI-SRTM assumes that BP_{ND} alters promptly from BP_{ND1} to BP_{ND2} at the time of the second injection and then remains constant. However, in reality this is unlikely and the binding condition of [^{11}C]raclopride may be continuously changed along time. In this simulation, the detectability of the reduction of BP_{ND} due to changes in binding conditions was investigated. Noiseless time–activity curves of the striatum and cerebellum were generated with a measured plasma TAC and assumed parameter values derived from measurements taken from the monkey study. A TAC of the cerebellum was simulated with a conventional two-tissue compartment, four-parameter model with assumed parameter values obtained previously in our monkey study: $K_1 = 0.034$, $K_1/k_2 = 0.36$, $k_3 = 0.022$, $k_4 = 0.034$. Meanwhile, a TAC of the striatum was simulated with an extended two-tissue compartment model

Please cite this article as: Ikoma, Y., et al., Quantitative evaluation of changes in binding potential with a simplified reference tissue model and multiple injections of [^{11}C]raclopride, NeuroImage (2009), doi:10.1016/j.neuroimage.2009.05.099

expressed as Eq. (3) by the fourth-order Runge–Kutta method (Endres et al., 1997).

$$\begin{aligned}
\frac{dC_f}{dt} &= K_1 C_p(t) - (k_2 + k'_3(t))C_f(t) + k_4 C_b(t) \\
\frac{dC_b}{dt} &= k'_3(t)C_f(t) - k_4 C_b(t) \\
k'_3(t) &= k_{on}\frac{B_{max} - \frac{C_b(t)}{SA}}{1 + D(t)} \\
D(t) &= B_1 \qquad (t<t_2) \\
&= B_2 + A \cdot \exp(-R(t - t_2)) \quad (t \geq t_2)
\end{aligned} \tag{3}$$

where C_f and C_b are the concentrations of radioactivity for free and specifically bound [^{11}C]raclopride in tissue, respectively; B_{max} is the total dopamine D_2 receptor concentration; k_{on} is the bimolecular association rate constant for raclopride; SA is the specific activity of administered [^{11}C]raclopride; D is the concentration of free dopamine. In this simulation study, t_2 was set to 30 min, and SA that was decay corrected to the first injection time was assumed to be equal in first and second injections with a single synthesis. Each assumed parameter for K_1 to k_4 was obtained from our monkey study, and the B_{max} value was as reported previously (Endres et al., 1997), thus $K_1 = 0.033$, $K_1/k_2 = 0.59$, $k_{on} = 0.0048$, $B_{max} = 17.6$; $k_4 = 0.026$; $B_1 = B_2 = 0$, and SA = 37 GBq/μmol at the time of first injection.

First, the magnitude of the BP_{ND} change, derived from an increase in released dopamine, was investigated. Time–activity curves, including dopamine release, were simulated from Eq. (3), in which A varied: 0.5, 1.0, 1.5 and 2.0, and R varied: 0.04, 0.07, and 0.1. In these simulated TACs, BP_{ND1} and BP_{ND2} were estimated by the MI-SRTM, and the relationship between the magnitude of the BP reduction ($\Delta BP = (BP_{ND1} - BP_{ND2})/BP_{ND1}$) and the integral of the dopamine pulse D in Eq. (3) was examined.

Next, the BP change caused by an increase in administered raclopride was investigated. $D(t)$ in Eq. (3) was set to 0, and tissue TACs were generated using the input plasma TAC in which administration of the first injection was assumed as 1 nmol raclopride, and the second injection was amplified from 1 to 50 times greater than the first injection. In these simulated TACs, BP_{ND1} and BP_{ND2} were estimated by the MI-SRTM, and the relationship between the magnitude of ΔBP and the amount of raclopride administered by the second injection was examined.

Effect of binding change timing on BP_{ND} estimates

It is possible that the change in BP_{ND} occurs either before, or after, the second injection of [^{11}C]raclopride. In the MI-SRTM, the error in the estimates for the first injection of [^{11}C]raclopride amplifies the errors in the estimates for the second injection. In this simulation, the effect of the onset of the dopamine pulse on the binding change of BP_{ND}, estimated by the MI-SRTM, was investigated using noiseless simulated TACs. First, TACs with a released dopamine pulse were generated using Eq. (3), with the parameters mentioned above, and three types of pulse ($A = 0.5$, $R = 0.1$; $A = 1.0$, $R = 0.07$; $A = 1.5$, $R = 0.04$) in which the onset time of the dopamine pulse, t_2 in Eq. (3), was changed from −10, −5, 0, 5, 10, 15 min against 30 min intervals of the second injection. The values for BP_{ND1}, BP_{ND2}, and ΔBP were estimated by the MI-SRTM, and the relationship between the onset time of the dopamine pulse and the BP_{ND} estimates was investigated.

Next, TACs were generated by the SRTM with measured cerebellum TACs and assumed parameter values ($R_1 = 0.86$, $k_2 = 0.091$, and $BP_{ND1} = 2.2$) using the fourth-order Runge–Kutta method, assuming a prompt change of BP_{ND} at −10, −5, 0, 5 and 10 min after the second injection (30 min intervals). The value of BP_{ND2} was also varied so that ΔBP would be 0, 10, 20, 30, 40, 50, 60, 70, and 80%. In these simulated TACs, BP_{ND1}, BP_{ND2}, and ΔBP were estimated by the MI-SRTM, and the estimated values were compared with the true values.

Effect of injection interval on BP_{ND} estimates

The relationship between the reliability of the BP_{ND} estimates from the MI-SRTM and the injection interval was investigated with noise-added TACs. A dynamic tracer concentration for [^{11}C]raclopride was derived from the equation of MI-SRTM (Eq. (2)) with a measured cerebellum TAC used as the input function and the rate constant values given as true values ($R_1 = 0.95$, $k_2 = 0.067$, $BP_{ND1} = 2.6$, $BP_{ND2} = 2.6$, 1.8, or 0.78) assuming a prompt BP reduction at the time of the second injection. The timing of the second injection was varied from 20 min to 90 min after the first scan.

The Gaussian-distributed mean-zero noise with variance proportional to the true count was added to the non-decaying tissue activity for each frame using Eq. (4) (Logan et al., 2001):

$$\sigma_i(\%) = 100 \cdot F / \sqrt{C_t(t_i) \cdot e^{-\lambda t_i} \cdot \Delta t_i} \tag{4}$$

where i is the frame number; C_t is the non-decaying tissue radioactivity concentration derived from the rate constants and the input function; t_i is the midpoint time of the i'th frame; Δt_i is the data collection time; λ is the radioisotope decay constant; F is a scaling factor representing the sensitivity of the measurement system, introduced here to adjust the noise level. It should be noted that this equation assumes that noise, which is added to the TAC, is determined by the count of the curve itself. In fact, noise is determined by the total counts in the slice, and is affected by random counts, dead time, etc. In this simulation study, F was set to 15.0 so that the noise level would be the same as the noise level for regions of interest (ROI)-based analysis, and 1000 noisy data sets were generated for each injection interval.

In these simulated TACs, BP_{ND1} and BP_{ND2} were estimated by the MI-SRTM, and estimated BP_{ND1}, BP_{ND2}, and ΔBP values were compared with the true values. Parameter estimates were considered outliers if either BP_{ND1} or BP_{ND2} was outside the range $0.0 < BP_{ND} < 10.0$. The reliability of the estimated parameters was evaluated by the mean and coefficient of variation (COV; SD/mean[%]) of the estimates excluding outliers, and the relationship between the reliability of the parameter estimates and the injection interval was investigated.

Monkey study analysis

Studies on monkeys with dual injections of [^{11}C]raclopride were performed to determine whether the present approach can estimate two identical BP_{ND} values when there is no change in binding conditions during the scan, and whether this approach can detect a change in BP_{ND} values when the binding conditions do change during the scan. The monkeys were maintained and handled in accordance with guidelines for animal research on Human Care and Use of Laboratory Animals (Rockville, National Institute of Health/Office for Protection from Research Risks, 1996). The study protocol was approved by the Subcommittee for Laboratory Animal Welfare of the National Cardiovascular Center.

First, PET studies were performed in four cynomolgus macaques (weight 3.6 ± 0.56 kg) by administering the same molar amount of [^{11}C]raclopride for the first and second injections (Table 1). Anesthesia was induced with ketamine (8.4 mg/kg, intramuscularly) and xylazine (1.7 mg/kg, intramuscularly) and maintained by intravenous propofol (6 mg/kg/h) and vecuronium (0.02 mg/kg/h) during the scan. Initially, 418 ± 111 MBq of [^{11}C]raclopride was administered by a bolus injection, and after 30 min, the same molar amount of [^{11}C]raclopride as for the first injection, was administered by a bolus

Please cite this article as: Ikoma, Y., et al., Quantitative evaluation of changes in binding potential with a simplified reference tissue model and multiple injections of [^{11}C]raclopride, NeuroImage (2009), doi:10.1016/j.neuroimage.2009.05.099

Table 1
Injection protocol in monkey studies with dual injections of [^{11}C]raclopride.

	Subject	Specific activity at the time of first injection [GBq/μmol]	Injection interval [min]	First injection		Second injection	
				Injected mass [nmol]	Injected activity at the time of first injection [MBq]	Injected mass [nmol]	Injected activity at the time of second injection [MBq]
	#1	64.9	30	8.4	548		198
	#2	75.2	30	5.9	444		160
Exp. 1	#3	29.3	30	13.6	399	Same as first injection	144
	#4	39.7	30	7.1	280		101
	mean ± SD	52.3 ± 21.4	30	8.8 ± 3.4	418 ± 111		151 ± 39.9
Exp. 2	#5	22.6	30	3.3	73.3	30.7	249

Exp. 1: Dual injections with same mass of [^{11}C]raclopride.
Exp. 2: Dual injections with different mass of [^{11}C]raclopride.

injection. Data were acquired for 60 min (10 s × 18, 30 s × 6, 120 s × 7, 300 s × 2 for the first injection; 10 s × 18, 30 s × 6, 120 s × 7, 300 s × 2 for the second injection). The specific radioactivity was 52.3 ± 21.4 GBq/μmol at the time of the first injection.

Next, PET studies were performed on a cynomolgus macaque (weight 6.0 kg) with the administration of different molar amounts of [^{11}C]raclopride for the first and second injections by changing the volume of second injection with [^{11}C]raclopride which was synthesized before the first injection (Table 1). For the first injection, a bolus of 73.3 MBq of [^{11}C]raclopride, (3.3 nmol of raclopride) was administered, and after 30 min, 249 MBq at the time of the second injection (decay corrected 691MBq) of [^{11}C]raclopride (30.7 nmol of raclopride) was administered by bolus injection. The specific radioactivity was 23 GBq/μmol at the time of the first injection.

PET scans were performed using a PCA-2000A positron scanner (Toshiba Medical Systems Corporation, Tochigi, JAPAN) that provides 47 planes and a 16.2 cm axial field of view. A transmission scan with a 3-rod source of ^{68}Ge–^{68}Ga was carried out for 20 min for attenuation correction before the administration of [^{11}C]raclopride. Radioactivity was measured in two-dimensional mode and the data were reconstructed by a filtered back-projection using a Gaussian filter (full width at half maximum is about 6.0 mm (Herzog et al., 2004)). VOIs were defined manually over the left and right striatum and cerebellum for PET images, and the radioactivity concentration in these regions was obtained. For each region, R_{11}, k_{21}, BP_{ND1}, R_{12}, k_{22}, and BP_{ND2} were estimated by MI-SRTM. In addition, parametric images were generated, estimating each parameter voxel by voxel, using the MI-SRTM with the basis function method.

Results

Detection of BP_{ND} change with dual-injection

Typical examples of simulated TACs in the dual-injection study with dopamine release are shown in Fig. 1. In the simulation studies, the magnitude of ΔBP, estimated by the MI-SRTM, was investigated in the two cases where the specific binding changed due to the released dopamine pulse or to an increase in administered raclopride. The magnitude of ΔBP increased as the integral of the dopamine pulse increased (Fig. 2A). To some extent there was a good linear correlation between the reduction in BP_{ND} and the integral of the dopamine pulse ($Y = 2.0*X + 2.3$, $R^2 = 0.95$ where $X < 15$ (X: Integral of the dopamine pulse, Y: reduction in BP_{ND})); however the relationship did not remain linear for a large dopamine pulse. The reduction in BP_{ND} also became greater when the injected mass of raclopride increased, although its relationship was nonlinear (Fig. 2B).

Effect of binding change timing on BP_{ND} estimates

In the simulation with a released dopamine pulse, when the dopamine pulse was released before the second injection, the BP_{ND1} value was underestimated and BP_{ND2} was overestimated, compared with the situation where the dopamine pulse was released at the same time as the second injection (Figs. 3A, B). On the other hand, when the dopamine pulse was released after the second injection, BP_{ND1} was unchanged and BP_{ND2} varied according to the onset and magnitude of the dopamine pulse. The reduction in BP_{ND} also depended on the

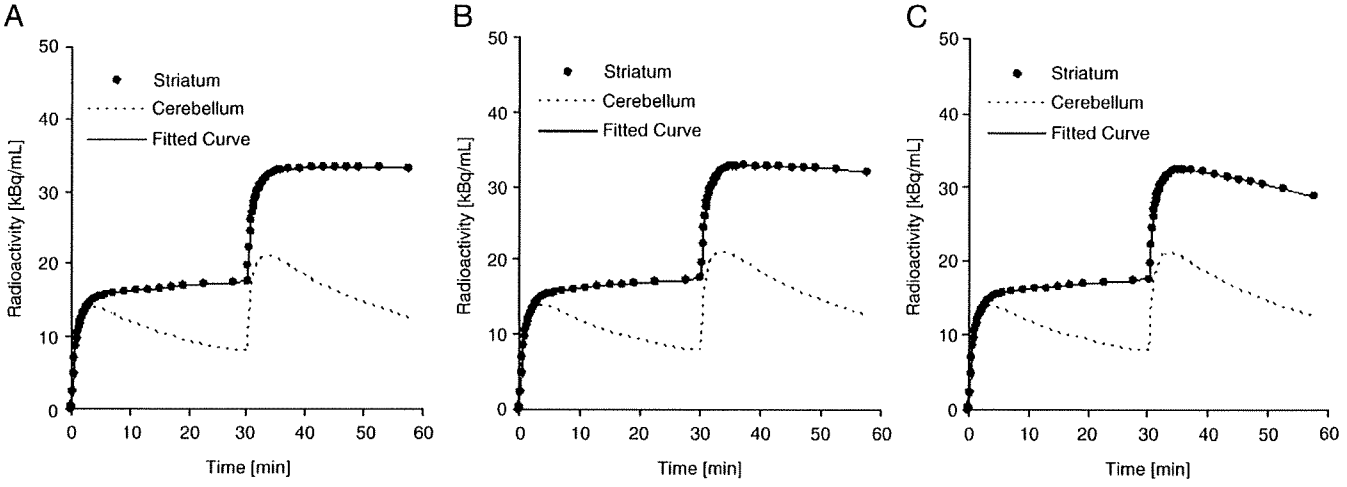

Fig. 1. Simulated time–activity curves for the striatum and cerebellum without dopamine pulse (A), with small dopamine pulse ($A = 0.5$, $R = 0.04$) (B), and with large dopamine pulse ($A = 1.5$, $R = 0.1$) (C), and fitted curve for the striatum by MI-SRTM.

Please cite this article as: Ikoma, Y., et al., Quantitative evaluation of changes in binding potential with a simplified reference tissue model and multiple injections of [^{11}C]raclopride, NeuroImage (2009), doi:10.1016/j.neuroimage.2009.05.099

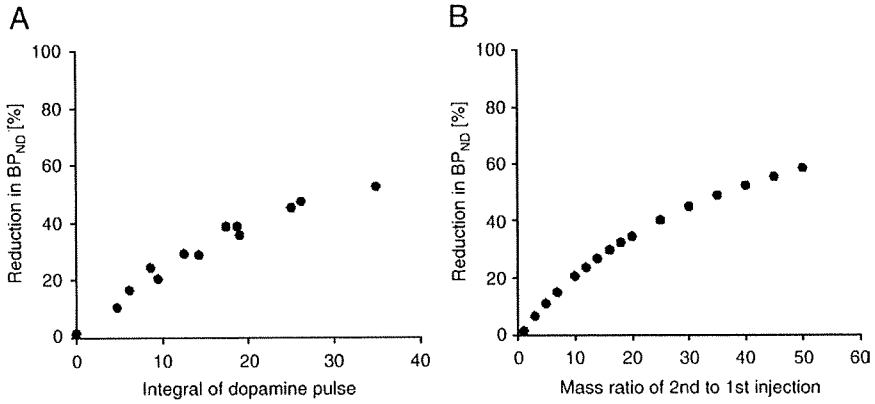

Fig. 2. Relationship between percentage reduction in BP_{ND} and the integral of the dopamine pulse in simulation studies in which dopamine was released at the same time as the second injection, performed 30 min after first injection (A); and the relationship between percentage reduction in BP_{ND} and the mass of the second injection in simulation studies in which a greater mass of raclopride was administered 30 min after the first injection.

onset, magnitude of amplitude, and decay rate of the dopamine pulse, and the reduction in BP_{ND} was greatest when the dopamine pulse was released 5 min after the second injection (Fig. 3C). When the magnitude of the dopamine pulse was small, the detected BP_{ND} reduction was small when the dopamine pulse was released before the second injection, becoming greatest (about 20%) when the pulse was released 5 min or 10 min after the second injection. When the magnitude of the pulse was medium, the BP_{ND} reduction was 20% when the pulse was released 5 min before the second injection, and it was greatest (about 35%) when the pulse was released 5 min after the second injection. When the dopamine pulse was large, the detected BP_{ND} reduction was 30% even when the pulse was released 10 min before the second injection, and was greatest (about 45%) when the pulse was released 0 or 5 min after the second injection.

In the simulation with prompt BP_{ND} reduction, BP_{ND1}, BP_{ND2} and ΔBP were estimated precisely by the MI-SRTM when the BP_{ND} reduction occurred at 30 min, in other words, at the same time as the second injection (Fig. 4). In the case where the BP decreased before 30 min, the estimated BP_{ND1} was lower than the true value for BP_{ND1} (=2.2), and the magnitude of the underestimation increased when the true BP_{ND2} was lower, that is to say, the reduction in BP_{ND} was greater (Fig. 4A). There were slight errors in BP_{ND2} estimates (Fig. 4B). When the BP_{ND} decreased 50% (BP_{ND1} = 2.2 and BP_{ND2} = 1.1) at 10 min before the second injection, estimated BP_{ND1} was 1.63 and BP_{ND2} was 1.04. Conversely, when the BP decreased after 30 min, BP_{ND1} was estimated precisely, and BP_{ND2} was overestimated (Figs. 4A and B). The error in BP_{ND2} estimates increased as the magnitude of the BP_{ND} reduction increased. When the BP_{ND} decreased 50% (BP_{ND1} = 2.2 and BP_{ND2} = 1.1) at 10 min after the second injection, estimated BP_{ND1} was 2.20 and BP_{ND2} was 1.28. With respect to the magnitude of the BP reduction, the estimated ΔBP was lower than the true value when the BP reduction was greater, or the difference between the timing of the BP_{ND} decrease and the second injection was greater (Fig. 4C). When the BP_{ND} reduction began 10 min before the second injection, the error in the estimated ΔBP was considerable. However, when the BP_{ND} reduction began, either 5 min before or 5 min after, the second injection, the error in ΔBP was less than 5% when the reduction in the BP was lower than 50%.

Effect of injection interval on BP_{ND} estimates

Errors in the estimated BP_{ND1}, BP_{ND2} and ΔBP values were investigated in simulated noise-added TACs for various injection intervals, and it was observed that the errors became larger as the injection interval became shorter (Fig. 5). The COVs of BP_{ND1} and BP_{ND2} were less than 5% and the bias was less than 1% when the injection interval was longer than 30 min, in both cases where the reduction in the BP_{ND} was 30% and 70%. When ΔBP was 30%, the bias increased suddenly, and the COV of ΔBP rose to over 10% for an injection interval of less than 40 min. There were no outliers even if the injection interval was 20 min. Meanwhile, when ΔBP was 70%, there was little bias and the COV of ΔBP was less than 10% for an injection interval longer than 30 min. The COV of ΔBP in the 70% reduction TAC was lower than that in 30% reduction TAC. However,

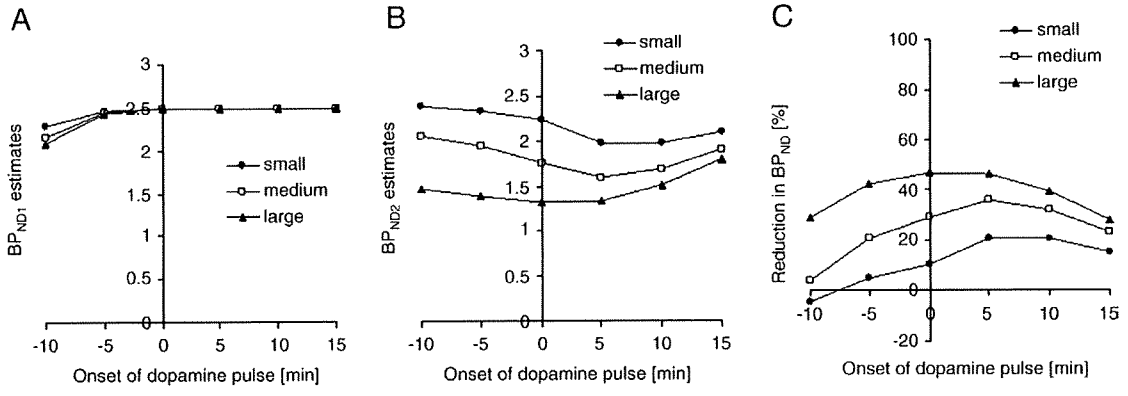

Fig. 3. Relationship between estimated values of BP_{ND1} (A), BP_{ND2} (B), reduction in BP_{ND} (C) and the onset of the dopamine pulse, in simulation studies with a small pulse (H = 0.5, R = 0.1), medium pulse (H = 1.0, R = 0.07), and large pulse (H = 1.5, R = 0.04) released −10, −5, 0, +5, +10, or +15 min with respect to the second injection.

Please cite this article as: Ikoma, Y., et al., Quantitative evaluation of changes in binding potential with a simplified reference tissue model and multiple injections of [^{11}C]raclopride, NeuroImage (2009), doi:10.1016/j.neuroimage.2009.05.099

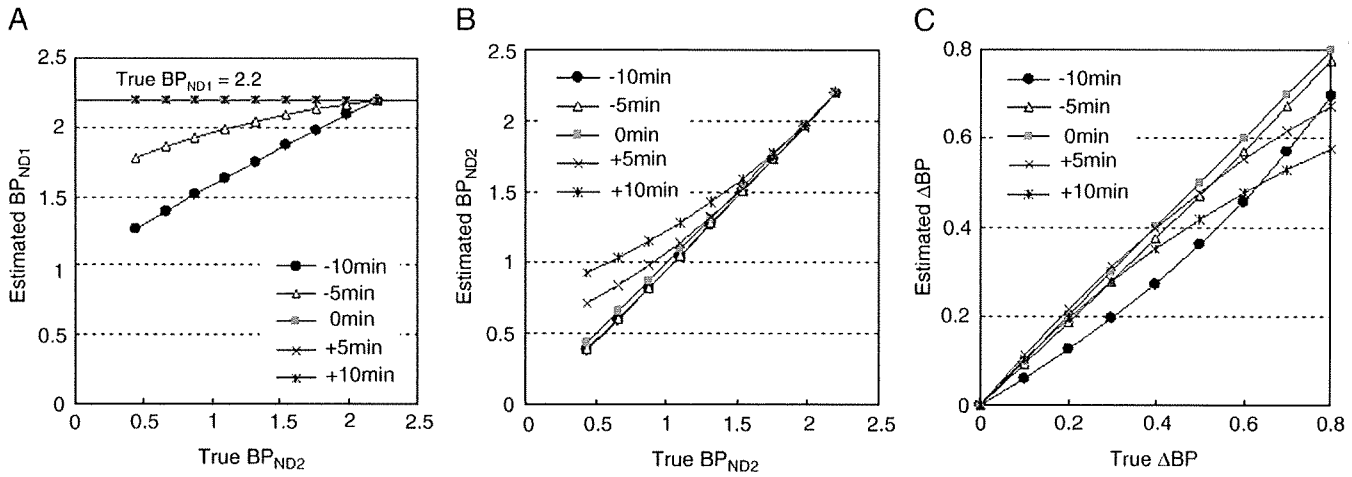

Fig. 4. Relationship between estimated values of BP_{ND1} (A), and BP_{ND2} (B) and the true values of BP_{ND2}, and the relationship between the estimated reduction in BP_{ND} (ΔBP) and true ΔBP (C) in the simulation studies in which BP_{ND} changed promptly from 2.2 to the true BP_{ND2} at −10, −5, 0, +5, or +10 min, with respect to the second injection.

there were 22 outliers with unreasonable estimates when the injection interval was 20 min and one outlier in one thousand estimates when the injection interval was 30 min.

Monkey studies

Typical examples of TACs for the striatum and the cerebellum in the dual-injection study with the same amount of raclopride are shown in Fig. 6. In these studies, the BP_{ND} values for the first and second injections could be estimated, and there were little differences between BP_{ND1} and BP_{ND2} (Table 2).

Time–activity curves for the striatum and the cerebellum in the dual-injection study using different amounts of raclopride are shown in Fig. 7, and the parametric images of BP_{ND1} and BP_{ND2} are shown in Fig. 8. The estimated BP decreased when the binding changed at the second injection due to the addition of more raclopride than was

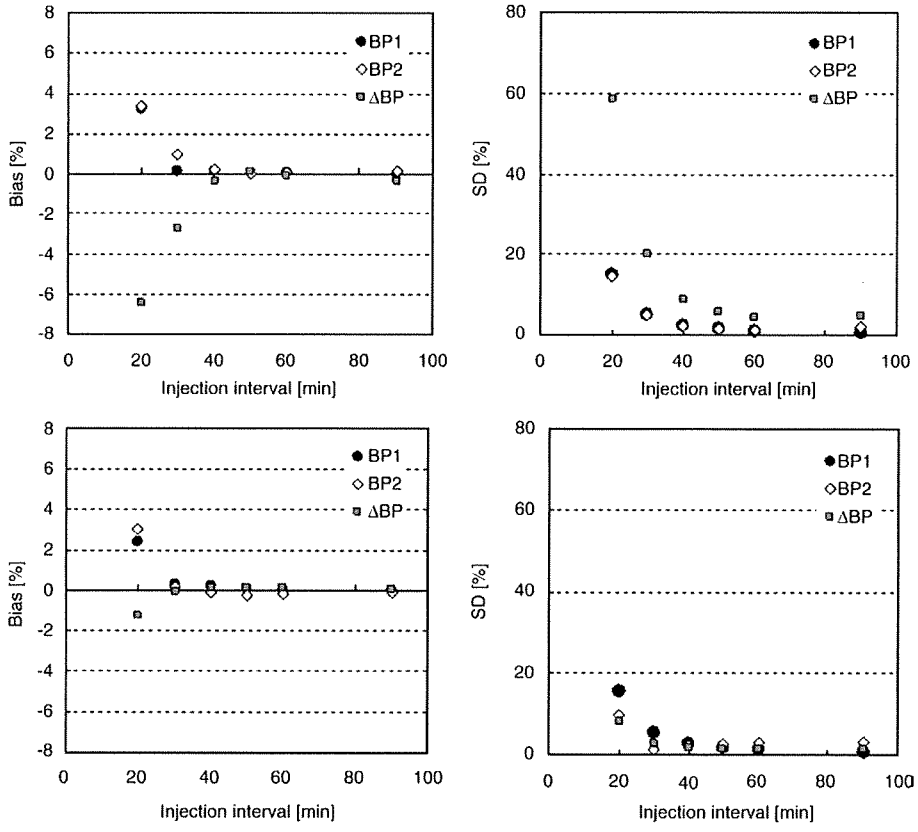

Fig. 5. Relationship between the injection interval and bias (left) or SD (right) of BP_{ND1}, BP_{ND2}, and the reduction in BP_{ND} (ΔBP) when BP_{ND} decreased by 30% (upper) or 70% (lower) at the time of second injection.

Please cite this article as: Ikoma, Y., et al., Quantitative evaluation of changes in binding potential with a simplified reference tissue model and multiple injections of [^{11}C]raclopride, NeuroImage (2009), doi:10.1016/j.neuroimage.2009.05.099

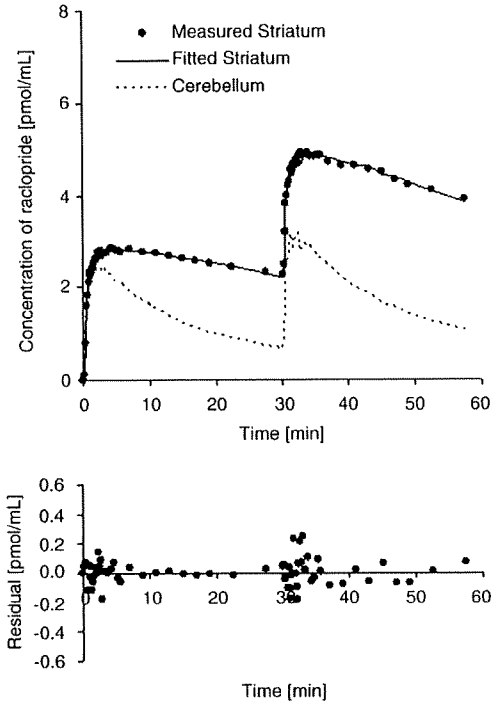

Fig. 6. Measured time–activity curves of the striatum and cerebellum in the dual-injection study with the same mass of [^{11}C]raclopride and a fitted curve for the striatum, using the multiple-injection SRTM (upper), and residuals between measured and fitted curves (lower).

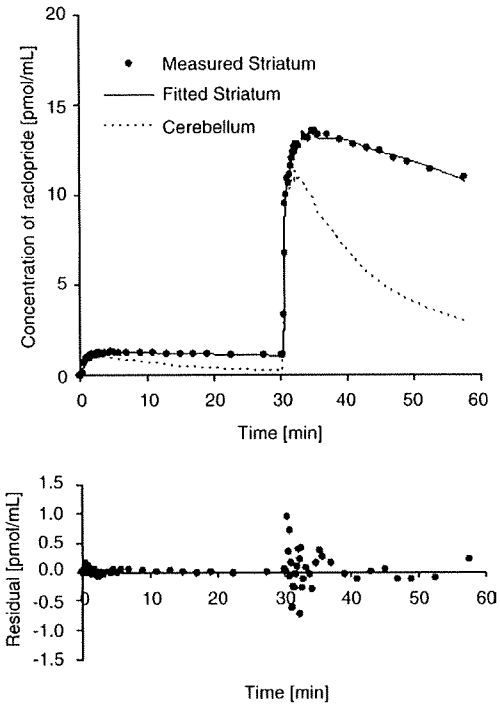

Fig. 7. Measured time–activity curves of the striatum and cerebellum in the dual-injection study with a different mass of [^{11}C]raclopride and a fitted curve for the striatum, using the multiple-injection SRTM (upper), and residuals between measured and fitted curves (lower).

administered for the first injection. Estimated BP_{ND1}, BP_{ND2} and ΔBP values in the striatum were 2.7, 2.0, and 25%, respectively (Table 2). The reduction in BP_{ND} was also observed in the parametric images as shown in Fig. 8.

Discussion

In the competition paradigm, the binding potential of [^{11}C] raclopride reflects the condition of specific binding to dopamine D_2 receptors, which is affected by competition with other ligands if there are no changes in the density of the receptors. The SRTM can provide the BP_{ND} value without invasive arterial blood sampling, using a TAC of the reference region, where specific bindings are negligible (Lammertsma and Hume, 1996), and this method has been widely used to estimate the binding of neuroreceptor ligands. However, in assessing temporal changes in the BP_{ND} of the SRTM caused by competition for receptor binding due to pharmacological administration or cognitive activation, multiple [^{11}C]raclopride PET scans are necessary and a long study period is required. To overcome this complication, we have proposed a multiple-injection approach in which the temporal change in BP_{ND} is quantified in a single scan with multiple [^{11}C]raclopride injections. This approach takes into account the residual radioactivity from the first injection in the target tissue, at the time of the second injection, as the initial condition in Eq. (2), and makes it possible to perform the second injection immediately, following data acquisition from the first injection. Thus it is possible to determine the change in BP_{ND} from a short study period.

There have been several investigators who attempted to perform multiple injections of ligands with PET studies for either obtaining receptor density and affinity by changing specific activity (Delforge et al., 1995; Millet et al., 1995; Morris et al., 1996a,b; Muzic et al., 1996; Christian et al., 2004; Gallezot et al., 2008), or obtaining different kinetic parameters simultaneously by injecting different tracers such as [^{11}C]flumazenil and [^{18}F]FDG (Ikoma et al., 2004; Koeppe et al., 2001). MI-SRTM gives us alternative approach for multiple-injection study which is aimed at shortening study period.

Table 2
Estimated BP_{ND1}, BP_{ND2}, and difference between BP_{ND1} and BP_{ND2} in monkey studies with dual injections of [^{11}C]raclopride.

	Subject	BP_{ND1}	BP_{ND2}	ΔBP
	#1	1.86	2.15	0.15
	#2	1.98	2.01	0.014
Exp. 1	#3	1.95	1.79	−0.081
	#4	2.33	2.39	0.027
	mean ± SD	2.03 ± 0.20	2.08 ± 0.25	0.029 ± 0.097
Exp. 2	#5	2.66	2.00	−0.25

$\Delta BP = (BP_{ND2} - BP_{ND1}) / BP_{ND1}$.
Exp. 1: Dual injections with same mass of [^{11}C]raclopride.
Exp. 2: Dual injections with different mass of [^{11}C]raclopride.

Detection of binding changes with the SRTM

In the multiple-injection approach, it is assumed that the change in binding conditions is reflected by a reduction in BP_{ND} estimated from the SRTM. The analysis method based on the compartment model assumes that the rate constants of K_1 to k_4 are constant during the scan. However, in studies with changes in binding conditions, levels of endogenous dopamine change after exposure to stimuli such as an amphetamine challenge (Endres et al., 1997; Laruelle et al., 1997), and the value of $k_3'(t)$ in Eq. (3) varies according to the concentration of free dopamine (Laruelle et al., 1997, Endres et al., 1997). Therefore, estimates of BP_{ND} following exposure to stimuli are considered to be an average value over time that is influenced by the dynamics of the neurotransmitter. However, it has been reported that reductions in BP_{ND}, estimated from graphical analysis or multilinear analysis, in simulation studies for two separate bolus-injection scans, are related to the integral of dopamine release (Endres and Carson, 1998; Yoder et al., 2004), and the reduction in BP_{ND} is a useful index for the evaluation of binding conditions in competition paradigms.

Please cite this article as: Ikoma, Y., et al., Quantitative evaluation of changes in binding potential with a simplified reference tissue model and multiple injections of [^{11}C]raclopride, NeuroImage (2009), doi:10.1016/j.neuroimage.2009.05.099

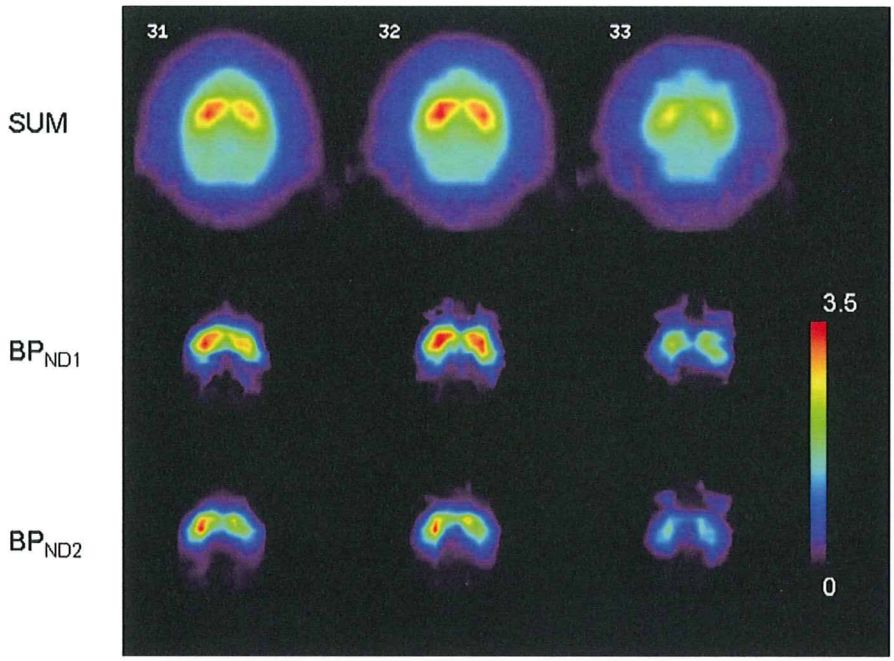

Fig. 8. Summation image and parametric images of BP_{ND1} and BP_{ND2} in the monkey study with dual injections of different masses of [^{11}C]raclopride.

In addition, in the SRTM, there are further assumptions that the target tissue and reference tissue can be expressed by a one-tissue compartment model, and the ratio of K_1 and k_2 are equal between the target and reference regions (Lammertsma and Hume, 1996). Strictly speaking, this assumption does not apply to [^{11}C]raclopride studies because significantly better fits were obtained with a two-tissue compartment model, as compared with those obtained with a one-tissue compartment model in cerebellum and striatum TACs (Lammertsma et al., 1996). Therefore, this assumption of the SRTM induces a bias in BP_{ND} estimates even in an ordinary single-injection study. In the MI-SRTM, which is an extension of the SRTM, the effect of the assumption could be more severe than for the SRTM because the bias in BP_{ND1} could be propagated to the estimation of BP_{ND2}. However, in our simulation studies, the ΔBP_{ND}, estimated from the MI-SRTM, increased according to the increase in the dopamine pulse or to administered raclopride (Fig. 2). When the specific binding of administered [^{11}C]raclopride competed with that of endogenous dopamine, to some extent the reduction in BP increased in proportion to the integral of the released dopamine pulse, and approached saturation as the integral of the pulse increased. This is consistent with results reported in previous studies (Endres and Carson, 1998, Yoder et al., 2004). Furthermore, in the monkey studies, it was confirmed that there was little change in BP_{ND} when the same mass of raclopride was administered for the first and second injections (Fig. 6), and the BP_{ND} decreased in accordance with the increase in administered raclopride (Figs. 7 and 8). Morris et al. (1996b) intensively investigated the characteristics of multiple injections PET studies, and they showed varied specific activity by multiple injections introduced bias in estimates of kinetic parameters. Our results may be influenced by the abrupt discontinuity in mass of raclopride due to the second injection. However, the result of second monkey study (10 times higher mass in the second injection) agreed well with the simulation (Fig. 2B) although further validation studies will be needed to confirm this result.

Effect of binding change timing on BP_{ND} estimates

In estimating the BP_{ND} after the dopamine pulse release, the timing of the [^{11}C]raclopride injection has been shown to affect the BP_{ND} estimates (Yoder et al., 2004). In the simulation study of our multiple-injection approach, BP_{ND1} (in other words, the BP_{ND} for the condition without dopamine activation) had few errors, except when the dopamine pulse was released 10 min before the second injection. In these simulations, BP_{ND1} was estimated using the data from the time interval between the first injection and the second injection. Therefore, when the BP_{ND} reduction, due to an increase in free dopamine, started before the second injection, the value for BP_{ND1} was underestimated. However, this underestimation can be avoided by adjusting the data points used for the fitting of BP_{ND1} so that BP_{ND1} is determined before a change in the binding conditions. On the other hand, BP_{ND2}, (that is to say, the BP_{ND} of the condition with dopamine activation) was affected by the timing of the dopamine pulse release. The estimated BP_{ND2} decreased as the onset of the dopamine pulse occurred later, and was smallest when the dopamine pulse was released 5 min after the second injection. As a result, the magnitude of ΔBP was greatest when the dopamine pulse was released 5 min after the second injection.

The value of $k_3'(t)$ in Eq. (3) depends upon the amount of free dopamine at time t (Endres et al., 1997, Endres and Carson, 1998) and the released dopamine pulse decreases as time goes by. Therefore, if the specific activity of administered [^{11}C]raclopride is high enough, the time-varying binding potential ($BPs(t) = k_3'(t)/k_4$) is lowest at the time of the pulse release, and it becomes greater, and approaches the level before the pulse release, as time passes. Meanwhile, the reduction in BP_{ND} is determined by both the $BPs(t)$ and the concentration of free tracer (Endres and Carson, 1998). In the TACs from our simulation studies, the concentration of free [^{11}C]raclopride had a peak at about 5 min after the injection, and ΔBP_{ND} was greatest when the onset of the dopamine pulse occurred 5 min after the injection, as shown in Fig. 3C. Therefore, the reduction in BP_{ND} was greatly affected, not only by the magnitude of the dopamine pulse, but also by its timing. In other words, if the kinetics of the free tracer are similar, that is to say the value of k_2 does not change markedly, and the timing of the dopamine release is the same, the estimated ΔBP changes according to the integral of the dopamine pulse as shown in Fig. 2.

In the situation where BP_{ND} changed promptly, the ΔBP_{ND} also depends upon the magnitude and timing of the BP_{ND} reduction. However, when ΔBP_{ND} was less than 40% and the time difference

Please cite this article as: Ikoma, Y., et al., Quantitative evaluation of changes in binding potential with a simplified reference tissue model and multiple injections of [^{11}C]raclopride, NeuroImage (2009), doi:10.1016/j.neuroimage.2009.05.099